Source details

Nuclear Engineering and Design

See also: Nuclear Engineering and Design/Fusion

Scopus coverage years: from 1965 to Present
Publisher: Elsevier
ISSN: 0029-5493

Subject area: Energy: Nuclear Energy and Engineering | Engineering: Safety, Risk, Reliability and Quality | Physics and Astronomy: Nuclear and High Energy Physics | Engineering: Mechanical Engineering | View all

Source type: Journal

CiteScore 2022
3.4

SJR 2022
0.853

SNIP 2022
1.234

View all documents > | Set document alert | Save to source list | Source Homepage

CiteScore | CiteScore rank & trend | Scopus content coverage

i Improved CiteScore methodology

CiteScore 2022 counts the citations received in 2019-2022 to articles, reviews, conference papers, book chapters and data papers published in 2019-2022, and divides this by the number of publications published in 2019-2022. Learn more >

CiteScore 2022

$$3.4 = \frac{\text{5,931 Citations 2019 - 2022}}{\text{1,734 Documents 2019 - 2022}}$$

Calculated on 05 May, 2023

CiteScoreTracker 2023

$$3.0 = \frac{\text{5,005 Citations to date}}{\text{1,660 Documents to date}}$$

Last updated on 05 August, 2023 • Updated monthly

CiteScore rank 2022

Category	Rank	Percentile
Energy — Nuclear Energy and Engineering	#27/68	61st
Engineering — Safety, Risk, Reliability and Quality	#76/192	60th

View CiteScore methodology > | CiteScore FAQ > | Add CiteScore to your site

Nuclear Engineering and Design

COUNTRY

Netherlands

Universities and research institutions in Netherlands

Media Ranking in Netherlands

SUBJECT AREA AND CATEGORY

Energy
- Nuclear Energy and Engineering

Engineering
- Mechanical Engineering
- Safety, Risk, Reliability and Quality

Environmental Science
- Waste Management and Disposal

Materials Science
- Materials Science (miscellaneous)

Physics and Astronomy
- Nuclear and High Energy Physics

PUBLISHER

Elsevier BV

H-INDEX

115

PUBLICATION TYPE

Journals

ISSN

00295493

COVERAGE

1965-2022

INFORMATION

Homepage

How to publish in this journal

Contact

SCOPE

Nuclear Engineering and Design covers the wide range of disciplines involved in the engineering, design, safety and construction of nuclear fission reactors. The Editors welcome papers both on applied and innovative aspects and developments in nuclear science and technology. Fundamentals of Reactor Design include: • Thermal-Hydraulics and Core Physics • Safety Analysis, Risk Assessment (PSA) • Structural and Mechanical Engineering • Materials Science • Fuel Behavior and Design • Structural Plant Design • Engineering of Reactor Components • Experiments Aspects beyond fundamentals of Reactor Design covered: • Accident Mitigation Measures • Reactor Control Systems • Licensing Issues • Safeguard Engineering • Economy of Plants • Reprocessing / Waste Disposal • Applications of Nuclear Energy • Maintenance • Decommissioning Papers on new reactor ideas and developments (Generation IV reactors) such as inherently safe modular HTRs, High Performance LWRs/HWRs and LMFBs/GFR will be considered; Actinide Burners, Accelerator Driven Systems, Energy Amplifiers and other special designs of power and research reactors and their applications are also encouraged.

Join the conversation about this journal

Quartiles

FIND SIMILAR JOURNALS

1
Hedongli Gongcheng/Nuclear Power Engineering
CHN
87%
similarity

2
Science and Technology of Nuclear Installations
EGY
85%
similarity

3
Journal of Nuclear Engineering and Radiation
USA
72%
similarity

4
Annals of Nuclear Energy
GBR
65%
similarity

5
Pro
GBI

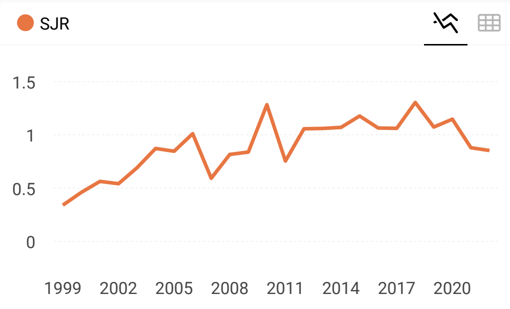

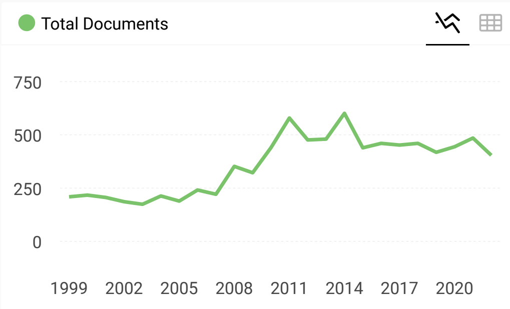

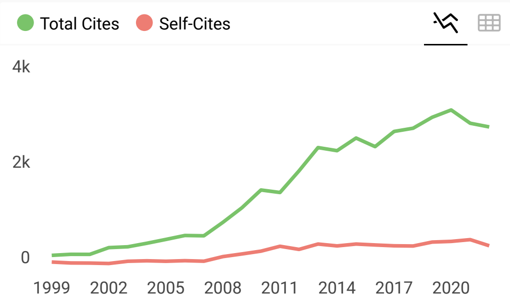

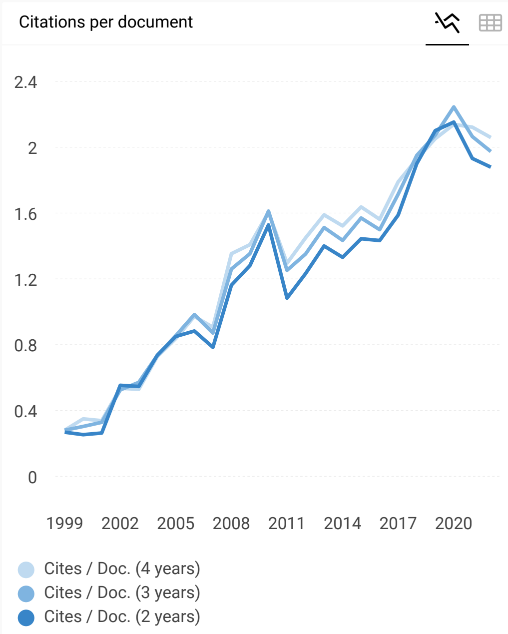

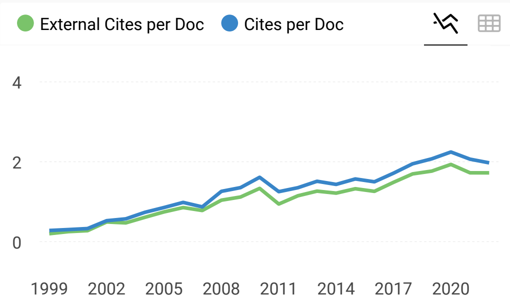

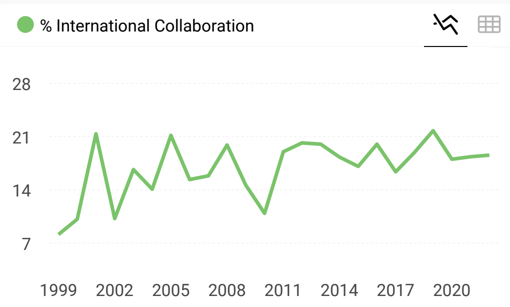

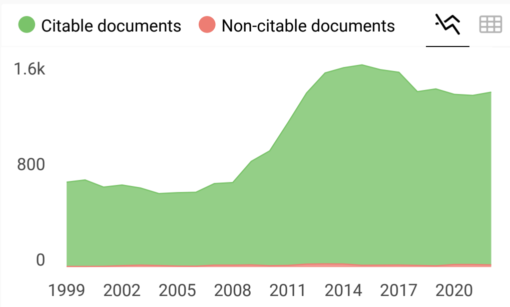

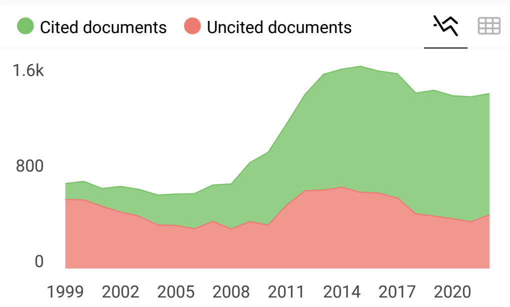

← Show this widget in your own website

Just copy the code below and paste within your html code:

<a href="https://www.scimag

VOLUME 412 OCTOBER 2023 ISSN 0029-5493

Nuclear Engineering and Design

An International Journal devoted to all aspects of Nuclear Fission Energy

Available online at www.sciencedirect.com

ScienceDirect

Affiliated with the European Nuclear Society (ENS) and with the International Association for Structural Mechanics in Reactor Technology, e.V. (IASMiRT)

Volume 399
1 December 2022

Full text access
Editorial Board

Article 112073

View PDF

Engineering Mechanics

Research article ○ Abstract only
Drag coefficient estimation in FSI for PWR fuel assembly bowing

L. Longo, K. Cruz, N. Cadot, E. Sarrouy, ... C. Eloy
Article 111995

Article preview

Research article ○ Abstract only
Simulation on the evaporative cooling characteristics of humid air-water outside staggered tube bundles

Siwen Tan, Xuefeng Wu, Hongqiang Ma, Yue Xie, ... Yufei Chen
Article 112028

Article preview

Material Properties

Research article ○ Abstract only
Statistical learning model for fuel-cladding heat exchange coefficient evaluation in SFR

Marlène Jeannin, Victor Blanc, Vincent Dupont, Vincent Pascal, ... Pablo Rubiolo
Article 112027

Article preview

Reactor Engineering

Research article ○ Abstract only
Development and validation of theoretical-computational model for nuclear powered hydrogen production: A case study for Saudi Arabia

Salah Ud-Din Khan, Abdullah Al-Hamdan, Zeyad Almutairi
Article 112018

Article preview

Research article ○ Abstract only

Design of data-driven model for the pressurizer system in nuclear power plants using a TSK fuzzy neural network

Tarek A. Mahmoud, Amal A. Sheta, Refaat M. Fikry, Elsayed H. Ali, ... Mohammed I. Mahmoud
Article 112015

Article preview

Research article ● *Open access*

On butterfly effect in the dynamics of Oskarshamn-2 instability event of 1999

Abdelhamid Dokhane, Alexander Vasiliev, Hakim Ferroukhi
Article 112016

View PDF Article preview

Fuel Engineering

Research article ○ Abstract only

The design from scratch to an alternative experimental assembly for the LVR-15 research reactor – A case study in Czech Republic

Vincenzo Romanello, Antonio Dambrosio, Jaroslav Ernest, Milos Kyncl, ... Cyrille Rontard
Article 112007

Article preview

Research article ○ Abstract only

Study on evaluation method of kernel migration of TRISO fuel for High Temperature Gas-cooled Reactor

Yuji Fukaya, Shoichiro Okita, Koei Sasaki, Shohei Ueta, ... Xing L. Yan
Article 112033

Article preview

Research article ○ Abstract only

LOCA advanced failure criteria: Implementation in the mechanistic fuel performance code and practical applications

M.S. Veshchunov, A.V. Boldyrev, V.E. Shestak
Article 112039

Article preview

Reactor Components

Research article ○ Abstract only

Experimental and numerical investigation of non-uniform inflow on cavitation characteristics of reactor coolant pumps

Yu Song, Song Huang, Rui Xu, Zhengchuan Zhang, ... Dezhong Wang
Article 112013

Article preview

Core Physics

Research article ○ Abstract only

Neutronics simulation of China Experimental Fast Reactor start-up tests using FARCOB and ERANOS 2.1 code systems

Abhitab Bachchan, K. Devan, A. Riyas
Article 112038

Article preview

Thermal Hydraulics

Research article ○ Abstract only

Effects of swirl intensity on interfacial and wall friction factors of annular flows in a vertical pipe

Ryoya Koto, Ryo Kurimoto, Atsuya Imaizumi, Kosuke Hayashi, Akio Tomiyama

Article 112001

Article preview

Research article ○ Abstract only

Improvement of GAMMA+ code for system transient and thermo-fluid safety analysis of sodium-cooled fast reactors

Nam-il Tak, Hong Sik Lim, Jonggan Hong, Jung Yoon, ... Jaehyuk Eoh
Article 112002

Article preview

Research article ● *Open access*

Numerical study on the thermal-hydraulic behavior in the ultimate heat sink of passive residual heat removal system in the SMART

Seong Dae Park, Dong Won LEE, Kyung Jun Kang, Hyun-Sik Park
Article 111997

View PDF Article preview

Research article ○ Abstract only

Optimization investigation on the distribution of both inlets and outlets for the shell of a novel separated structure steam generator

Huaishuang Shao, Jian Jiao, Shifeng Deng, Qinxin Zhao, ... Yungang Wang
Article 112000

Article preview

Research article ● *Open access*

Analysis of sodium boiling initiated by unprotected loss of flow in European sodium fast reactor core with different subassembly designs

J. Bodi, A. Ponomarev, K. Mikityuk
Article 112014

View PDF Article preview

Research article ○ Abstract only

A Lagrangian approach to ex-vessel corium spreading over ceramic and concrete substrates using moving particle hydrodynamics

Ryo Yokoyama, Masahiro Kondo, Shunichi Suzuki, Michael Johnson, ... Koji Okamoto
Article 112029

Article preview

Research article ○ Abstract only

Hydraulic design optimization of spherical header for future fast reactors of India

Amit K. Chauhan, M. Rajendrakumar, K. Natesan
Article 112017

Article preview

Research article ○ Abstract only

Validation of the STEG code using experiments on Two-Phase flow across horizontal tube bundles

Shixian Liu, Fei Yin, V.I. Melikhov, O.I. Melikhov
Article 112048

Article preview

Research article ○ Abstract only

An experimental study on the effect of liquid properties on the counter-current flow limitation (CCFL) during gas/liquid counter-current two-phase flow in a 1/30 scaled-down of Pressurized Water Reactor (PWR) hot leg geometry

Achilleus Hermawan Astyanto, Indarto, Karen Vierow Kirkland, Deendarlianto
Article 112052

Article preview

Safety and Risk Analysis

Research article ○ Abstract only

Study on structural integrity of reactor pressure vessel with various ablation under core meltdown accident

Anyu Liao, Jiadong Yang, Ting Jin, Pan Liu, ... Jianfeng Mao
Article 111999

Article preview

Instrumentation and Control

Research article ○ Abstract only

Dependability analysis of safety critical and control systems of NPP

Raj Kamal Kaur, Lalit Kumar Singh, Pooja Singh
Article 112031

Article preview

Experiments

Research article ○ Abstract only

Experiments on the localized interaction at the interface fuel rod/spacer grid in pressurized water reactors

Giovanni Ferrari, Kostas Karazis, Marco Amabili
Article 111998

Article preview

New Reactor Concepts

Research article ○ Abstract only

Multi-physics coupling analysis on neutronics, thermal hydraulic and mechanics characteristics of a nuclear thermal propulsion reactor

Zimian Duan, Jing Zhang, Yingwei Wu, Binqian Li, ... G.H. Su
Article 112042

Article preview

Technical Note

Short communication ○ Abstract only

A complementary study on the thermophysical and gas-dynamic characteristics of a hybrid fusion–fission reactor facility during operation

A.V. Arzhannikov, S.V. Bedenko, V.V. Prikhodko, V.M. Shmakov, ... H.R. Vega-Carrillo
Article 112037

Article preview

Special Section on "Advanced Topical Meeting on Advanced in Thermalhydraulics 2020 (ATH'20)"; Edited by: Dr. Sofiane Benhamadouche and Prof. Igor Bolotnov

Editorial ○ No access

Foreword to “Advanced Topical Meeting on Advanced in Thermal Hydraulics 2020 (ATH’20) Special Issue”

Article 111996

Special Issue On "NURETH-19"; Edited by: Dr. Elia Merzari, Ir. Ferry Roelofs, Dr. Philippe Planquart, and Dr. Katrien Van Tichelen

Research article ○ Abstract only

Validation of URANS and STRUCT-ε turbulence models for stratified sodium flow

Ralph Wiser, Emilio Baglietto, James Schneider, Mark H Anderson
Article 112009

Article preview

Research article ○ Abstract only

Advanced Thermal-Hydraulic experiments and instrumentation for heavy liquid metal reactors

Julio Pacio, Katrien Van Tichelen, Sven Eckert, Thomas Wondrak, ... Toshinobu Sasa
Article 112010

Article preview

Research article ○ Abstract only

Iterative computed tomography reconstruction of void fraction in a fuel bundle on unstructured mesh

Jean-Marie Le Corre
Article 112008

Article preview

Research article ○ Abstract only

Application of the depth-averaged liquid film model to the annular flow regime in BWR fuel assemblies

Chidambaram Narayanan, Emeline Beltjens, Rita Szijarto, Dionysios Chionis, Christian Hellwig
Article 112003

Article preview

Research article ○ Abstract only

Scaled validation test for high prandtl number fluid mixed convection between parallel plates

Floren Rubio, Nicolas Zweibaum, Ian Craig, Johnathan Gilbreth, ... Haihua Zhao
Article 112006

Article preview

Research article ○ Abstract only

Status of benchmark exercises in the frame of the NUGENIA QUESA project

T. Hollands
Article 112011

Article preview

Research article ○ Abstract only

3D field data of flow structures in dead-ended, coolant loop reactor branch lines for CFD validation of thermal fatigue onset modeling

J.R. Downing, V. Petrov, A. Manera
Article 112012

Article preview

Research article ○ Abstract only

Turbulent heat flux modelling in forced convection flows using artificial neural networks

Matilde Fiore, Lilla Koloszar, Miguel Alfonso Mendez, Matthieu Duponcheel, Yann Bartosiewicz
Article 112005

Article preview

Research article ○ Abstract only

Development of machine learning framework for interface force closures based on bubble tracking data

Cheng-Kai Tai, Ilya Evdokimov, Fabian Schlegel, Igor A. Bolotnov, Dirk Lucas
Article 112032

Article preview

Research article ○ Abstract only

PAR model development exercise in the framework of SAMHYCO-NET

E.-A. Reinecke, J. Fontanet, L.E. Herranz, Z. Liang, ... S. Gupta
Article 112035

Article preview

Research article ○ Abstract only

Analysis of air ingress scenario in GEMINI+ plant

M.M. Stempniewicz, E.A.R. de Geus, F. Roelofs, M. Skrzypek, ... C. Pohl
Article 112030

Article preview

Research article ○ Abstract only

High-fidelity pool boiling simulations on multiple nucleation sites using interface capturing method

Yuqiao Fan, Mengnan Li, William D. Pointer, Igor A. Bolotnov
Article 112004

Nuclear Engineering and Design 399 (2022) 112052

Contents lists available at ScienceDirect

Nuclear Engineering and Design

journal homepage: www.elsevier.com/locate/nucengdes

An experimental study on the effect of liquid properties on the counter-current flow limitation (CCFL) during gas/liquid counter-current two-phase flow in a 1/30 scaled-down of Pressurized Water Reactor (PWR) hot leg geometry

Achilleus Hermawan Astyanto [a,c], Indarto [a,b], Karen Vierow Kirkland [d], Deendarlianto [a,b,*]

[a] Department of Mechanical and Industrial Engineering, Universitas Gadjah Mada, Jalan Grafika No 2 Kampus UGM, Yogyakarta 55281, Indonesia
[b] Center of Energy Studies, Universitas Gadjah Mada, Sekip K-1A Kampus UGM, Yogyakarta 55281, Indonesia
[c] Department of Mechanical Engineering, Universitas Sanata Dharma, Kampus III USD Maguwoharjo, Yogyakarta 55282, Indonesia
[d] Department of Nuclear Engineering, Texas A&M University, 3133 TAMU College Station, TX 77843-3133, USA

ARTICLE INFO

Keywords:
PWR hot leg
CCFL
Liquid properties
Dimensional analysis

ABSTRACT

To promote the safety of the nuclear reactors, numerous authors have carried out investigations of gas/liquid counter-current two-phase flow in order to understand the characteristics during the inception of flooding or CCFL. The present work covers an experimental and analytical study on the effect of liquid properties on CCFL characteristics in a complex geometry representing 1/30 scaled-down version of a German-Konvoi PWR hot leg. The obtained results reveal that the gas velocity to initiate the flooding monotonically decreases with the increase of the liquid velocity. At high liquid flow rates, it is noticed that with the increase of glycerol percentage, the gas flow rate needed to initiate the flooding significantly decrease due to either the increase in liquid viscosity or the decrease in corresponding surface tension. Here under the same flow condition, the flooding is initiated faster by the higher glycerol percentage. Moreover, instead of the well-known Wallis superficial velocity, the Kutateladze-type parameter or a combination of the Wallis parameter and liquid property numbers by Zapke & Kröger (1996) which were previously proposed by numerous authors to investigate the effects of liquid properties on CCFL characteristics, a modified non-dimensional Wallis parameter combined with the inverse viscosity number introduced by Ma et al. (2020) is found herein to more accurately correlate the present experimental data. Through a dimensional similarity analysis, a new empirical correlation reveals that the liquid Froude number is the greatest determinant of CCFL characteristics with respect to the effect of the liquid properties.

1. Introduction

In a hypothetical scenario during the operation of pressurized water reactor (PWR) power plant, which is widely known as small break loss-of-coolant-accident (SBLOCA), vaporization takes place due to depressurization of the coolant water in the reactor primary circuit. This saturated steam due to depressurization along with steam due to core decay heat flow from the reactor vessel (RV) into the steam generator (SG) via a channel, namely hot leg. In a type of German-Konvoi PWR, this conduit comprises a horizontal pipe and an inclined pipe connected by an elbow. A fraction of the steam condenses in the U-tube steam generator tubes, and under the action of gravity, the generated condensate flows back through the hot leg to the RV, counter-currently with the steam. As the density of the condensate is higher than that of the steam, a stratified layer occurs in the hot leg in which the condensate is underneath the steam.

The counter-current flow of steam and condensate is stable only for certain ranges of the fluid flow rates. Once the gradually increasing steam flow rate exceeds, a maximum velocity to maintain counter-current flow, the onset of flooding, which is also known as counter-current flow limitation (CCFL), occurs. A further increase of the steam flow rate causes the vapor-liquid interface to be unstable. The condensate is partially entrained, and these entrained droplets may reverse flow direction to travel co-currently with the steam. Additional increase of the steam flow rate results can cause complete flow reversal of the liquid

* Corresponding author at: Department of Mechanical and Industrial Engineering, Universitas Gadjah Mada, Jl. Grafika No 2, Yogyakarta 55281, Indonesia.
E-mail address: deendarlianto@ugm.ac.id (Deendarlianto).

https://doi.org/10.1016/j.nucengdes.2022.112052
Received 6 September 2022; Received in revised form 26 October 2022; Accepted 6 November 2022
Available online 12 November 2022

Nomenclature

Symbols

J_K	Phase superficial velocity (m/s)
J_K^*	Phase Wallis parameter (-)
ρ_K	Phase density (kg/m^3)
μ_K	Phase dynamic viscosity (kg/m.s)
σ_L	Liquid surface tension (N/m)
Re_K	Phase Reynolds number (-)
Ku_K	Phase Kutateladze number (-)
We_K	Phase Weber number (-)
g	Gravitational acceleration (m/s^2)
D	Channel diameter (m)
R^2	Coefficient of determinant (-)
Z_L	Liquid property parameter (-)
N_L	Inverse viscosity number (-)
Bo	Bond number (-)
Fr_K	Phase Froude number (-)
W_K^*	Modified Wallis parameter combined with inverse viscosity number (-)

phase and water cannot return to the RV (Deendarlianto et al., 2012).

Due to the importance of comprehensive knowledge of the critical conditions leading to CCFL, the present works investigates the effect of liquid properties on CCFL characteristics through extensively experimental database to assess the significance of non-dimensional groups employed for CCFL correlation. An empirical correlation to predict the flooding gas velocity in the corresponding geometry incorporating the effect of liquid properties is also addressed in conjunction with theoretical modeling to develop necessary and sufficient groups of non-dimensional numbers to correlate the CCFL. However, since the flow conditions that impede natural circulation limit the adequate core cooling under postulated accident in light water reactor systems, comprehensive knowledge of flooding phenomenon is of interest and essential for establishing appropriate accidental management strategies (Vierow et al., 2015). Therefore, an extensive understanding of the role of liquid property allows for better accuracy in analysis to promote extended operation and improve the reactor safety (Deendarlianto et al., 2010).

1.1. Previous research on CCFL and fluid properties

Over the years, a large number of studies on counter-current flow have been conducted to understand the fundamental aspects of CCFL mechanisms and characteristics in accordance with the safety design of nuclear reactors. Extensive research data, particularly on the basis of experimental investigations, have been tabulated and acquired under diverse conditions. The conditions are imposed either by the test section, i.e., geometrical aspects governing the CCFL, or the interfacial behaviors due to the test condition, i.e., applied flow parameters (Murase et al., 2012). In addition, the influence of the fluid properties on CCFL characteristics have been also investigated, but has received less attention. Fluid property studies include the effects of the fluid viscosity (Clift et al., 1966; Suzuki & Ueda, 1977; Zapke & Kröger, 1996; Ghiaasiaan et al., 1997; Mouza et al., 2003; Kinoshita et al., 2011; Prayitno et al., 2012; Kusunoki et al., 2015) as well as the influences of the liquid surface tension (Deendarlianto et al., 2004; 2010; Ousaka et al., 2006; Kinoshita et al., 2011) on the CCFL characteristics. Furthermore, those accumulated data have also resulted in the developments of empirical correlations covering various parameters to predict CCFL (Deendarlianto et al. 2012).

Regarding the effect of the liquid viscosity, the earliest experimental study to measure the flooding gas velocities in wetted wall columns was reported by Clift et al. (1966). Water and aqueous glycerol solutions were utilized as the test liquid during the experiment while air was employed as the gaseous phase. Water-glycerol solutions were employed because the viscosity could be specified while maintaining a fluid with Newtonian behavior. The wetted wall columns were comprised of two Perspex tubing, 31.75 mm of diameter and 1.83 in length. Next, Suzuki & Ueda (1977) examined the liquid film behaviors during CCFL in a vertical pipe. The test section was made from transparent acrylic with 28.8 mm of diameter and 1.83 m of length. To measure the maximum thickness of the liquid film, a contact probe was employed which was acquired by 1 kHz of a sampling rate. Moreover, the interaction between waves on liquid film and air stream was further taken into account during the CCFL characterizations.

Subsequently, Zapke & Kröger (1996) carried out an experimental investigation on the effect of fluid physical properties on the CCFL characteristics. Here, a 30 mm inner diameter pipe made of transparent acrylic was utilized as the test section. The air, argon, helium and hydrogen were utilized as the gaseous phase, while water, methanol, isopropanol and aqueous methanol solutions were the tested liquids. To correlate the obtained experimental data, an improved CCFL empirical model was proposed. Moreover, a series experimental study on the influence of fluid properties was conducted to identify the flow pattern through pressure drop characteristics in rectangular conduits (Zapke & Kröger, 2000a). The tested fluids also utilized water, methanol, propanol as the liquid phase while air, helium, hydrogen and argon were used as the gaseous phase. In addition, the validity of the Froude-Ohnesorge parameter representing the CCFL characteristics was assessed using several previously results by a number of authors (Zapke & Kröger, 2000b). Here, the general validity of the non-dimensional groups was also exhibited by utilizing several previous reports.

Another steady-experimental investigation on the hydrodynamic characterizations on the effects of liquid properties on both vertical and inclined counter-current two-phase flow was carried out by Ghiaasiaan et al. (1997). The test section was a transparent acrylic pipe with 1.9 cm of inner diameter and 2 m of channel length of pipe. Several water-based solutions comprised of demineralized water, mineral and paraffinic oils were employed as the liquid medium while air was utilized as the gaseous phase. On the other hand, Mouza et al. (2003) investigated the effect of liquid properties on CCFL in inclined small diameter pipes. Here, the tested liquids were water and kerosene, while air was utilized as the gaseous phase. Furthermore, the characteristics of the liquid film were taken into account on the interpretation of the obtained flooding data, in which the superficial Reynolds numbers were divided into several distinct ranges describing different observed phenomena obtained during the experiment. Of interest to the current work, Drosos et al. (2006) reported an experimental investigation of the effect of liquid properties on CCFL under relatively low liquid Reynolds numbers. The test section was a rectangular duct with a 70 cm high and 12 cm wide made of a Plexiglas material. An amount of air was employed as the gaseous phase while the liquid was varied by the percentage of butanol. In this study, the test liquid with the highest concentration of glycerol will be shown to have a low Reynolds number and a distinct CCFL trend.

Exhibiting specific attention on the effect of the liquid surface tension, an investigation of the flow patterns and CCFL characteristics in an inclined pipe was reported by Deendarlianto et al. (2004). The channel, made of transparent acrylic, was 16 mm in diameter and 5.5 m in length. Water-based solutions were employed as the liquid phase whereas air from compressor was utilized as the gaseous phase. A type of surfactant, namely oleic acid natrium, was employed to obtain three variations of the liquid with different surface tension without altering the other properties, i.e. the density and viscosity. Three pairs of liquid holdup array probes were employed by constant electric current method. The obtained experimental data were plotted as flow pattern maps comprising the CCFL in terms of the superficial velocity, Wallis parameter, Froude-Ohnesorge number, and also Webber number

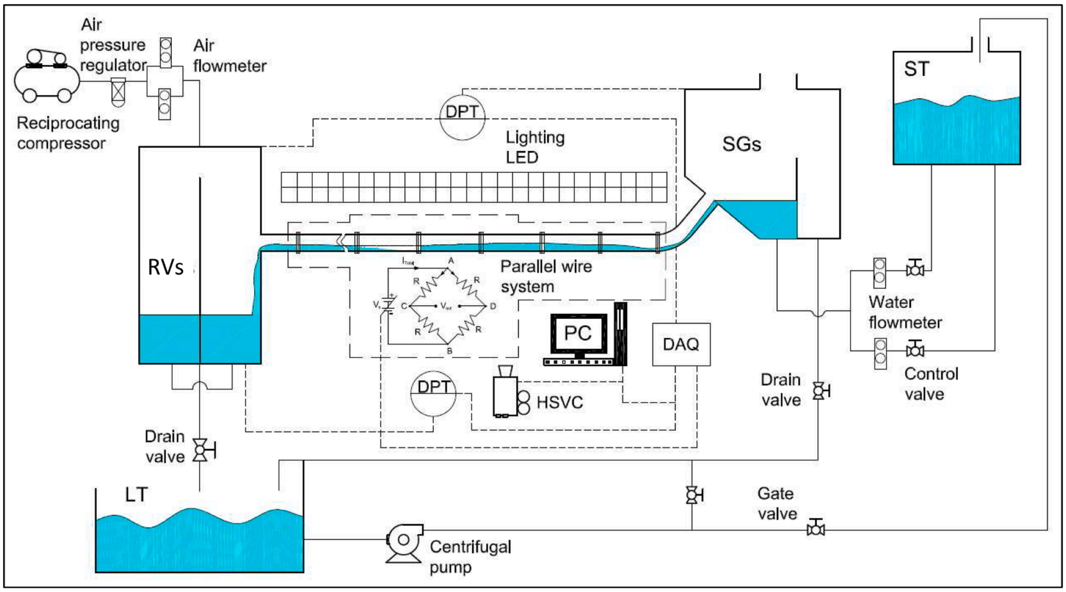

(a) Schematic diagram (Astyanto et al., 2022)

(b) Test section

Figure 1. The schematic diagram of the experimental apparatus (a) and test section (b).

comprising both the liquid and gaseous phase, respectively. Furthermore, the wave breakdown location, well known as the locus was proposed through both visualization and signal processing of the time variation of liquid-holdup as partial flooding characteristics (Deendarlianto et al., 2010). In addition, Ousaka et al. (2006) proposed a new correlation to predict the flooding gas velocity which was developed on the basis of the obtained experimental data considering the effect of surface tension as a part of fundamental parameters on the flooding gas velocity.

Due to the fact that varying a certain fluid property without altering other properties is a problematic aspect during the experiment in which a small variation in the remaining properties may causes another considerable effect, several authors decided to conduct their flooding experiments considering the influence of both the viscosity and surface tension of the medium liquid. Here, Kinoshita et al. (2011) carried out both numerical and experimental studies which were focused on the effects of liquid properties on the CCFL characteristics in a scaled-down model of a PWR hot leg. A pipe with 50 mm of cross section diameter and 430 mm of horizontal length representing a 1/15-scale model of the German-Konvoi hot leg was utilized as the test section. The glycerol-water solutions were employed as the liquid phase while air was used as the gaseous phase. Furthermore, a numerical based study was also embedded to support the investigation on the interfacial drag coefficient dynamics caused by the change of the liquid viscosity towards the CCFL characteristics. On the other hand, Prayitno et al. (2012) conducted an experimental investigation on the effect of liquid properties on CCFL characteristics in nearly horizontal channels. The test section utilized a 50 mm inner diameter tube that was 1.1 m in length and made of a transparent acrylic material. On the other hand, various water-based solutions, comprised of glycerol and butanol, were employed as the liquid phase while the gaseous phase utilized air from a compressor. The obtained data were plotted in CCFL curves in terms of phase superficial velocity, phase Wallis velocity and also modified Wallis parameter which was also previously employed by Zapke & Kröger (1996).

From the above literature surveys, extensively dedicated experimental data of the hot leg geometries have been carried out utilizing various scale models. We further notices that the obtained data have been being correlated due to the different aspects between the test facilities and the real PWR conditions. However, the conditions of those facilities may also differ one from another. Here, a large number of authors reported using atmospheric pressure during their experiments, whereas, the real primary circuit engages at higher system pressures. Consequently, this discrepancy in the pressure condition affects the physical properties of the medium fluids. The higher the pressure, the larger the viscosity, and the smaller the surface tension of the saturated water. Therefore, from the aforementioned surveys, it is revealed that CCFL characteristics depend on the liquid properties. Subsequently, it is strongly recommended that those extensive data should be reassessed given the significance of non-dimensional groups employed for general correlation (Mouza et al., 2003) due to insufficient data taken under prototypical conditions leading to CCFL that still exists in the literatures (Drosos et al. 2006).

A number of authors have proposed various non-dimensional groups to correlate the flooding data even though they only correlate their own data without assessing applicability of the correlations to the other authors data (Zapke & Kröger, 2000b). Therefore, a comprehensive correlation that accounts for all of the aforementioned effects during the counter-current flow should be pursued to engage those effect of fluid properties change (Kinoshita et al., 2011). A large number of correlations to predict the CCFL have also been proposed, but most include considerable uncertainties which indicates the limitations of those correlations (Prayitno et al., 2012).

Assessment of the state of knowledge of CCFL from the myriad of past studies reveals that correlation developments on the basis of experimental data to predict the flooding gas velocity is of considerable importance since a predictive capability for CCFL requires an extensive experimental data base (Siddiqui et al., 1986). The developments of necessary and sufficient groups of non-dimensional numbers to correlate the CCFL data must be pursued in conjunction with theoretical modeling (Deendarlianto et al., 2010).

To the authors' knowledge, empirical correlations to predict the effect of liquid properties on the flooding gas velocity are limited to a straight geometry covering either inclined or vertical conduit. Complex geometries representing models of PWR hot leg receive still smaller attention. Therefore, the present work also addresses an empirical correlation development to predict the flooding gas velocity during counter-current flow in a 1/30 scaled-down model of a PWR hot leg incorporating the effect of liquid properties.

2. Experimental apparatus and procedures

The present work covers an experimental study on the effect of liquid physical properties on the CCFL in a geometry representing PWR hot leg. The experiment facility has been developed in the Fluid Mechanics Laboratory of Universitas Gadjah Mada, Indonesia. It supports the experiments utilizing 1/30 scaled-down model of the German Konvoi type of hot leg with a circular cross section. The continuous development is during a multiphase flow research framework which has previously covered several investigations on counter-current flow investigations on the basis of both signal and image data processing (Badarudin et al., 2016; Badarudin et al., 2018a; Badarudin et al., 2018b; Astyanto et al., 2021a; Astyanto et al., 2021b; Astyanto et al., 2022). Instead of PVC pipe, elastic rubber materials for the hoses are utilized in order to minimize the risk of leaking in both the liquid and gas supply systems. Thanks to the efforts, it also still delivers a relatively constant reading liquid flow rate into SGs as good as using the previous.

Moreover, the facility provides three liquid outlet from the upper liquid container. Therefore, every outlet is connected to a single water supply channel with a control valve installed. On the other hand, an outlet is also provided for liquid bypass to fasten the cycle time in the experimental running. Subsequently, instead of a conventional stopwatch, a time application (operated by android phone) enhanced with voice notes was applied. The timer installed on the smartphone was organized at the background so the times are able to be captured and included during the video recording. It pursues the chance to verify the delay between the signal and video recording through the visualizations. To optimize the lighting, beside the background, a spotlight at about 45 degrees of its direction to the test section was added. This enhances more the lighting intensity for visualization purpose in flow observations.

Furthermore, the prepared test section comprises the combination of a horizontal and an inclined channel which is connected by an elbow. The diameter of the test section is 25.4 mm, while the length of the horizontal and inclined pipe are 635 mm and 100 mm, respectively, with 135^{o} of an inclination angle. They were made of transparent acrylic resin. Figure 1(a) diagrammatically depicts the experiment facility reproducing the primary circuit of the PWR, a completely similar arrangement of experimental apparatus previously utilized by Astyanto et al. (2022) to investigate the statistical characterization of the interface fluctuations, while Figure 1(b) shows the test section.

The present experimental facility comprises both the main components and also supply system of the working fluids, a gas and a liquid. The main components contain a hot leg model exhibiting parallel wire array probes, a steam generator (SG) simulator and also a reactor vessel (RV) simulator. Ten pairs of silver plated copper wire with 0.4 mm and 5 mm in diameter and gap, respectively, are positioned normally to the liquid flow. Each pair exhibits a distance of 20 mm, and were installed to measure the interface fluctuations along the horizontal pipe. The SG simulator as well as the hot leg model were constructed from transparent acrylic. It aims to allow both the visual and optical observations during the investigation of the flow phenomena, directly, or by capturing the video image by the camera recorder. Meanwhile, the RV simulator was made from transparent glass. This coincides to visual observations toward the water level inside the RV simulator. Besides, a relatively thick glass material is intended to establish an appropriate strength vessel to prevent it from damage causing by the pressure during the experiments. Moreover, the detailed geometries of those main components are provided by Astyanto et al. (2022).

Table 1
Fluid physical properties obtained by in-house measurements

Fluid	Index	Density (kg/m^3)	Dynamic viscosity (kg/m.s)	Surface tension (N/m)
Air	-	1.15	1.87×10^{-5}	-
Distilled water	DW	977.34	7.97×10^{-4}	0.072
Distilled water + 25%wtGlycerol	G25	1030.19	17.17×10^{-4}	0.066
Distilled water + 40%wtGlycerol	G40	1058.13	31.67×10^{-4}	0.064
Distilled water + 50%wtGlycerol	G50	1088.52	54.23×10^{-4}	0.062
Distilled water + 60%wtGlycerol	G60	1126.34	95.72×10^{-4}	0.058

Table 2
Typical instrumentation

Instrument	Type	Specification
Gas flowmeter	Dwyer RMA	0–70 lpm (4% measurement error)
Liquid flowmeter	Dwyer RMB	0–20 gph (3% measurement error)
PT	Validyne P55D	86 kPa (0.25% measurement error)
	Validyne P55D	54 kPa (0.25% measurement error)
DAQ	Advantech 4716AE	200 kS/s; 16-bit; 16 channels
HSVC	Phantom Miro LAB310	3200 fps at maximum resolution

The flooding experiments were carried-out using air and five tested liquids as the fluid media. The liquid was varied by the concentration of glycerol. The temperature and pressure of the liquid corresponded to ambient conditions, and the relevant physical properties are given in Table 1. From the table it can be noticed that the effect of the glycerol concentration on liquid properties is primarily on the viscosity. Density changes by less than 15% and surface tension by less than 20% between pure distilled water and distilled water with the maximum glycerol concentration of 60%wt. The viscosity changes by about 120%, therefore dominating the effect of fluid property variations.

Dwyer model RMB flow meters were employed to measure the liquid flow rate at the liquid supply system. The calibration of the liquid flow meters was conducted by measuring the volume of liquid passed in a certain time range. The present method of the liquid flowmeter was previously employed by Clift et al. (1966). Dwyer model RMA flow meters were employed to measure the air flow rate at the gas supply systems. The air flow meters were calibrated by passing the air flow through the merit while another standard air flowmeter was connected in order to correlate the reading flow rate. The previous method was early employed by both Clift et al. (1966) and also Deendarlianto et al. (2011). Table 2 provides the description of the measurement instrumentations and their error reading which were used during the data tabulation.

The experiment is described as follows. An amount of liquid was pumped from the lower tank (LT) to the supply tank (ST) by using a pump. From the ST, due to the gravity acceleration, downwardly the liquid flows through a selected conduit, and filled the SG simulator. The liquid flow rate was adjusted using a control valve while its magnitude was read from the flowmeter which was installed on the supply pipe system. In a meantime, air from a compressor was introduced from RV simulator through the test section. To adjust the pressure and the gas mass flow rate, an air pressure regulator, ensuring unperturbed air flow (Choi & No, 1995), and air flowmeters were utilized, respectively. Here, the gas flow rate was controlled by the flowmeter's tuner which were parallel installed in the gas supply system.

The flooding experiments were carried out by adjusting and keeping the liquid flow rate as a constant variable, while the gas flow rate was stepwise increased with a small increment within the point in which the onset of flooding was reached. Deendarlianto et al. (2012) clearly noticed that during the counter-current flow, increasing the gas flow rate stepwise with a small increment under a constant liquid flow rate led to the flooding. This also agrees to the counter-current flow experiment which was previously conducted by Wongwises (1996) in which the onset of flooding was determined by keeping the injected liquid flow rate constant and the air flow rate was stepwise increased until the CCFL was reached, and further increased in order to reach the ZP to the RV simulator.

To confirm the repeatability of the data, partial experiments under the same test conditions were carried out. The subsequent experiments showed that the flooding points determined by a constant gas flow obtained were identical to those obtained during the constant liquid flow rate experiments. Moreover, the visual observations and the pressure drop data acquisitions were performed to obtain the flooding characteristics in which certain condition, the CCFL was reported to depend on the injected liquid flow rate. Subsequently, the liquid flow rate was stepwise increased to obtain several points of the onset of flooding with respect to the liquid flow rate change. In addition, several curves comprising the non-dimensional numbers were presented to describe the CCFL characteristics which strongly represents the relationship between the gas and liquid flow rates.

The interfacial behaviors during the counter-current flow were visually observed. From the observations, the visual data of the counter-current flow were also recorded by using a high speed video camera (HSVC). It comprised the flow developments and its corresponding phenomena, i.e., the flow regimes, hydraulic jump (HJ), subcritical and supercritical flow, wave development, etc. Here, the conceptual analysis involves visual observations of the flow structures, and the curve fitting on the basis of several non-dimensional parameters which were also utilized by a large number of authors. Furthermore, the raw data exhibit the optical objects as the high-quality videos describing the phenomena lead to the flooding characteristics. In addition, to obtain time-series signals of the fluctuation of the pressure differences between the SG and RV simulator, a pressure transducer (PT) was employed. Meanwhile, the water level in the RV simulator was also observed through a measurement line, and validated by signals acquired employing another PT. Those pressure probes were empowered by 12 VDC power adaptors and connected to an analog to digital converter data logger (DAQ) which was connected to a personal data storage computer. Subsequently, those data were acquired with 1 kHz of a sampling rate.

3. Results and Discussion

3.1. CCFL characteristics of the present experimental data in terms of existing group of non-dimensional numbers

The characteristics of counter-current flow limitation (CCFL) are often graphically described as the relation between the phase superficial velocities when a limit of the stability of the counter-current flow is reached before the liquid is carried over by the gas and partially entrained in the opposite direction (Vallée et al., 2011). The definition of the limitation may represent the maximum mass flow rate of the gas in which the discharge liquid flow leaving the channel is equal to the liquid flow rate in the inlet (Deendarlianto et al., 2012). Here, the CCFL is often visually determined through the first appearance of liquid flow reversal accompanied by either sharp rise of pressure drops or higher pressure

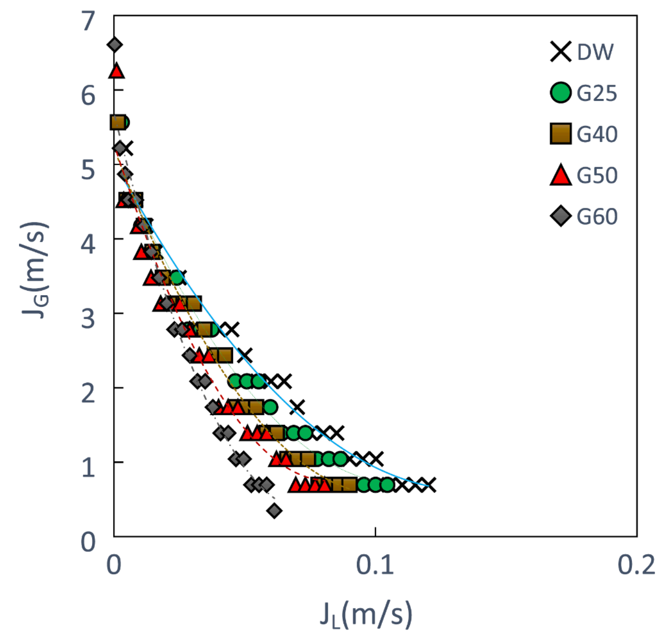

Figure 2. The CCFL characteristics in terms of phase superficial velocities

fluctuations in the channel due to the blockage of the gas flow by the liquid (Clift et al., 1966; Mouza et al., 2003, Deendarlianto et al., 2011; Vallée et al., 2012; Badarudin et al., 2018b). In addition, Zapke & Kröger (1996) earlier noticed that Diehl & Koppany (1969) as well as Chung et al. (1980) also defined the CCFL in terms of that similar determination, i.e., an abruptly increase in pressure drop across the conduit. Moreover, assessing the significance of non-dimensional numbers corresponding to the CCFL characteristics' investigations, we briefly describe the present experimental data of CCFL curve in several terms of those dimensionless corresponding numbers. The present manner has been successfully employed by Zapke & Kroger (1996; 2000b) and also Mouza et al. (2003) as well as Ma et al. (2020) in which it may elucidate either the influence of either the liquid properties or the channel diameters on CCFL characteristics.

In the present work, the experimental data are firstly plotted in term of a dimensional CCFL characteristic utilizing the phase superficial velocities (J_K). The present term has also been conducted by several of the mentioned authors. Here the present data exhibit that the critical gas superficial velocity or flooding gas velocity (J_G) decreases with the increase of the liquid superficial velocity (J_L) for the entire tested liquids' employed in the experiments. Furthermore, in the higher liquid flow rates, the change of the gas flow rate to initiate flooding tends to smaller. The higher the liquid flow rate, the smaller the change of the gas flow rate to obtain the CCFL. In several higher liquid flow rates, it is also revealed that an equivalent gas flow rate is able to initiate the flooding. Nevertheless, a gas flow rate seems to exhibit the CCFL of several liquid flow rates. It further implies a significance of the gas flow rate change to reach the CCFL towards the liquid flow rate. The CCFL characteristic curve in terms of phase superficial velocity for the present experimental data is depicted in Figure 2.

In addition, it is also obviously noticed from the curve that at a higher liquid flow rate, a smaller incremental increase in the gas velocity leads to the onset of flooding. This trend applies to all glycerol concentrations. It means that the higher the liquid flow rate, the more significant effect of liquid property's change on the CCFL. Here, the CCFL tends to be reached faster for the liquid with the higher glycerol percentage, or, the flooding gas velocity decreases with the increase in the glycerol percentage of the test liquid. Therefore, it can be clearly seen that the higher the glycerol concentration, the shallower the slope of the curve. The obtained curves which monotonically decline with an increase in the glycerol percentage represents the liquid properties exhibit a clear trend and effect. Taken from Suzuki & Ueda (1977), the present result is in an extensive agreement to the report by Clift et al. (1966) in which the flooding gas velocity reduces with the increase of liquid viscosity (μ_L), as a result of increasing the glycerol percentage under a constant liquid flow rate. Besides, the present result also implies a partial agreement to those experimental findings which were previously reported by Zapke & Kröger (2000a), Kinoshita et al. (2011) and also Prayitno et al. (2012) during the investigation of the effect of the liquid viscosity on the CCFL. As earlier published also by Chung et al. (1980), the liquids with the higher viscosity flood at low gas flow rates (Zapke & Kröger, 2000b). This trend is further confirmed by numerical studies reported by Utanohara et al. (2012) and also Pratama et al. (2021).

From the aforementioned findings, as reported by Zapke & Kröger (1996), and also Kinoshita et al. (2011), the physical explanations which are possible to be mapped out is that in the two phase flows, the shear force between the channel's wall and the liquid is strongly affected by the liquid viscosity. Here, the increase in the liquid viscosity, which mainly corresponds to the increase in the glycerol's percentage, affects the shear force between the fluid and the wall, especially in the high liquid flow rates. As the viscosity increases the shear force between the wall and the liquid increases. It further probably causes the amount of the falling liquid reduces (Kusunoki et al., 2015). On the other hand, the flooding is then also reported to be very close to the phenomenon of a drag in which the liquid weight is counter-balanced by the drag force exerted by the gas flow (Zapke & Kröger, 1996), even though Kinoshita et al. (2011) later suggested that the liquid viscosity affects the wall friction instead of the interfacial drag force. In addition, Prayitno et al. (2012) elaborated their findings to the previous findings in which the increase in the liquid viscosity corresponds to the increase in the flow resistance. Here, during the liquid flow, the pressure of the liquid film decreases as a result of the friction, while the pressure difference on the interface increases. This leads the interface to fluctuate due to the compensation of the pressure change on the fluid interface. Moreover, the liquid flowing in the conduit declines as the liquid viscosity decreases as early reported by Clift et al. (1966) during the investigation of the influence of the fluid viscosity on the vertical CCFL.

Empirically, during the characterization of the CCFL, both the fluid properties and flow parameters are mostly proposed to be correlated in terms of a group of dimensionless phase superficial velocity $\left(J_K^*\right)$, well known as the Wallis velocity, elaborating a balance of inertia and hydrostatic forces (Kang et al., 1999). Deendarlianto et al. (2012) noticed that Wallis (1961) successfully initialized a dimensionless parameter representing a modification of the Froude number, which is also defined as the ratio of inertia to buoyancy force and formulated as expressed in Eq.(1). Here also, in accordance with the density ratio, the fluid densities due to the pressure have been taken into account by the Wallis velocity (Vallée et al., 2012). Therefore, even though this non-dimensional number was originally proposed during a CCFL investigation in the vertical pipes, numerous authors have also extensively employed this parameter to characterize their CCFL data utilizing the inclined as well as the horizontal conduit, or even a complex geometry comprises horizontal and inclined section connected by an elbow representing a PWR hot leg. Accordingly, the CCFL characteristics may be correlated as expressed in Eq.(2).

$$J_K^* = J_K\left(\frac{\rho_K}{gD(\rho_L-\rho_G)}\right)^{0.5} \tag{1}$$

$$\left(J_G^*\right)^{0.5} + m\left(J_L^*\right)^{0.5} = C \tag{2}$$

Here in the Eq.(1) and Eq.(2), the subscription K represents the gas (G) or liquid (L) phase, while ρ denotes the fluid density, g stands for the gravitational acceleration, and D corresponds to the channel diameter. Furthermore, the constant m and C were determined by experimental

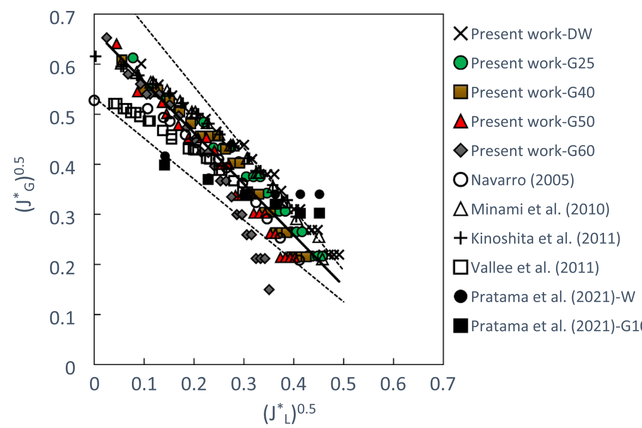

Figure 3. The CCFL characteristics in terms of non-dimensional square root of phase Wallis parameters

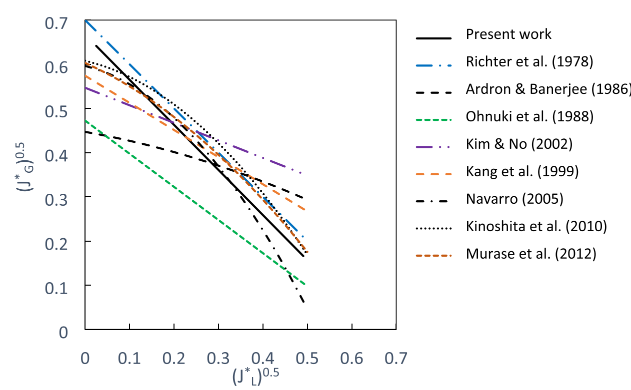

Figure 4. Comparison of the present correlation to several others which were previously obtained by other authors who also employee the Wallis parameter to reveal CCFL characteristics in the typical hot leg geometries

data in which there is no theoretical basis was derived for the use of the above correlation.

Figure 3 exhibits the curve of CCFL characteristics in terms of dimensionless square root of phase Wallis velocity. From the figure, it is clearly noticed that the gas flooding velocity decreases with the increase in the glycerol's percentage of the test liquid. On one hand, considering that the increase in the percentage of glycerol affects the liquid surface tension decreases, this might be further interpreted that the lower the liquid surface tension, the faster the flooding is initiated. Thus the present result is in a fair agreement to what previously reported by Deendarlianto et al. (2004; 2010) and also Ousaka et al. (2006) during the investigation of the effect of surface tension on CCFL in inclined pipes. On the other hand, calling that the viscosity increases with the increase of glycerol percentage, this could later satisfy such results as described in the previous passages in which the flooding gas velocity declines with the increase of the liquid viscosity.

As a comparison, several results obtained by Navarro (2005), Minami et al. (2010), Kinoshita et al. (2011), Vallée et al. (2011), and also Pratama et al. (2021) are also included in the graph employing the Wallis superficial parameter. It can be seen from the figure that the comparison exhibits an agreement to the present data in which the gas flow needed to initiate the flooding decreases as the liquid flow increases. Here, data from Navarro (2005), Minami et al. (2010), Kinoshita et al. (2011), Vallée et al. (2011) were obtained through experimental studies. On the other hand, Pratama et al. (2021), whose it case study was taken from the same facility scaling, i.e. 1/30-scale, carried-out a simulation study using Ansys Fluent.

Moreover, since the Wallis correlation may also be intended to

Table 3
Geometrical designations on several works in PWR hot leg typical CCFL

Authors	D(mm)	Scale	L/D	I/D	θ(deg.)	Cross section	P(MPa)	Fluid medium
Richter et al. (1978)	203.2	1/3.7	4.5	0	45	Circular	0.1	Air/water
Ardron & Banerjee (1986)	Theoretical modelling							
Ohnuki (1986)	Varied; 25.4	1/30	9.1	1.2	50	Circular	Varied	Air/water; steam/water
Kang et al. (1999)	Varied					Circular	0.1	Air/water
Kim & No (2002)	Varied					Circular	0.1	Air/water
Navarro (2005)	Varied; 54	1/15	9.3	1.9	50	Circular	0.1	Air/water
Kinoshita et al. (2010)	50	1/15	8.6	1.2	50	Circular	0.1	Air/water-glycerol
Murase et al. (2012)	Numerical simulation							
Present work	25.4	1/30	24	1.9	50	Circular	0.1	Air/water-glycerol

comprise the effect of viscosity (Suzuki & Ueda, 1977), therefore, applying 20% of relative deviation band, the present experimental data are also match the applied boundary, excepted several data obtained from G60 in the range of $(J_L^*)^{1/2} > 0.5$. Accordingly, through a linear regression with a 0.8785 of coefficient determinant/R-square (R^2), the experimental data invite a formula as written in Eq.(3).

$$(J_G^*)^{0.5} + 1.0207(J_L^*)^{0.5} = 0.667 \tag{3}$$

A plot of flooding diagram employing the Wallis velocity has been being common to describe a meaningful comparison of the experimental CCFL data (Vallée et al., 2012). Therefore, Figure 4 illustrates the comparison of the present data represented by Eq.(3), to several data which were previously obtained by other authors who also employee the Wallis parameter to reveal the CCFL characteristics. Here, those authors reported their experimental data on the predictions of the gas flooding velocity during the counter-current flow in the PWR hot leg typical geometries. The proposed correlations by Richter et al. (1978), Ardron & Banerjee (1986), Ohnuki (1986), Kang et al. (1999), Kim & No (2002), Navarro (2005), Kinoshita et al. (2010), and also Murase et al. (2012) expressed by either a linier or quadratic polynomial equation, respectively, are formulated as written in Eqs.(4) to (11). (Ardron & Banerjee, 1986) (Ohnuki, 1986) (Kang et al., 1999) (Kim & No, 2002) (Navarro, 2005) (Kinoshita et al., 2010) (Murase et al., 2012)

$$(J_G^*)^{0.5} + (J_L^*)^{0.5} = 0.7 \tag{4}$$

$$(J_G^*)^{0.5} + 0.263(J_L^*) + 0.176(J_L^*)^{0.5} = 0.447 \tag{5}$$

$$(J_G^*)^{0.5} + 0.75(J_L^*)^{0.5} = ln\left\{\left(\frac{L_H}{D}\right)\left(\frac{1}{L_I}\right)\right\}^{-0.066} + 0.88 \tag{6}$$

$$(J_G^*)^{0.5} + 0.397(J_L^*)^{0.5} = 0.603 - 0.00234\left(\frac{L_H}{D}\right) \tag{7}$$

$$(J_G^*)^{0.5} + 0.614(J_L^*)^{0.5} = 0.635 - 0.00254\left(\frac{L_H}{D}\right) \tag{8}$$

$$(J_G^*)^{0.5} + 1.71(J_L^*) + 0.2452(J_L^*)^{0.5} = 0.5963 \tag{9}$$

$$(J_G^*)^{0.5} + 1.28(J_L^*) + 0.238(J_L^*)^{0.5} = 0.608 \tag{10}$$

$$(J_G^*)^{0.5} + 0.81(J_L^*) + 0.45(J_L^*)^{0.5} = 0.63 \pm 0.03 \tag{11}$$

In addition, Figure 4 depicts the carried out comparisons. From the figure it can be seen that the present correlation, expressed by a linear equation, obtains a larger slope than the empirical correlations proposed by Kang et al. (1999) and Kim & No (2002), also in linier expressions. Furthermore, an almost similar slope to the empirical correlation by Richter et al. (1978) is observed, but the correlation by Richter et al. (1978) over predicts the present data. On the other hand, the correlation by Ohnuki (1986) largely underestimates the present data. Additionally, Ardron & Banerjee (1986), Navarro (2005), Kinoshita et al. (2010), and also Murase et al. (2012) proposed the CCFL correlation in a quadratic equation, respectively. Here, Ardron & Banerjee (1986) proposed a theoretical approaches considering a case with an ideal frictionless in the vertical to horizontal elbow while Kinoshita et al. (2010) carried out a numerical study.

Accordingly, from the figure it is clearly revealed that the comparison shows that there is a clear trend in which the gas velocity to initiate the flooding monotonically decreases with the increase of the corresponding liquid velocity. However, the distinguished slopes of the curves may correspond to the difference in either geometry or the fluid employed. For an instance, the scaling model and L/D which were utilized are different one to another. Here, except Ohnuki (1986) whose the model scale utilized was the same as the present experiment, i.e. 1/30 scaled-down geometry, the other investigators used the larger scales of hot leg models. Furthermore, in the perspective of the tested fluids, Richter et al. (1978), Kang et al. (1999), Kim & No (2002), and also Navarro (2005) employed a pair of air/water. Meanwhile, Kinoshita et al. (2010) utilized pairs of both air/water and steam/water in several scale models and also system pressures. Table 3 describes the geometrical aspects and medium fluid from the previous data which are compared to the present work.

Generally, the differences on the CCFL characteristics obtained by extensive authors have been reported to be affected by various aspects, i.e., the difference in model scale as well as the channel geometry, also system pressure and the fluid physical properties. The difference in scaling model might correspond to the significance effect of the fluid density to the stratified layer just before the CCFL. Here, the effect of density obtains the larger influence for the larger scaling model and/or channel diameter, while in the small diameter, the surface tension exhibits stronger effect. The larger diameter invites the lower drag force at the interface. Furthermore, the drag force affects the obtained liquid holdup in which the higher the drag, the larger the liquid holdup, and the smaller available area of the gas flow. Therefore, the smaller the gas flow area exhibited by the higher the drag force, the easier the breakdown of wave is obtained. As a result, the incipient of flooding occurs at a lower gas flow rate in which the liquid holdup increases as either the channel is longer (Ousaka et al., 2006), or the surface tension decreases (Deendarlianto et al., 2010).

Moreover, Al Issa & Macian-Juan (2014) reported that the diameter affects the interfacial area and the contact of the fluid, mainly for the liquid with the wall which further results on the interfacial force, the friction and also the surface tension. However, during the counter-current flow, the gravity force, parallel to the flow direction and opposed by the interfacial shear generated by the rather high gas velocity as well as the wall shear stress, regulates the liquid flow, while the surface tension and gravity force component perpendicular to the flow direction exert a stabilizing effect on the waves caused by the increase on gas flow rate (Mouza et al., 2003). Additionally, the viscous force is also reported to be gradually more active with the decline in channel diameter due to its dependency on both the viscosity coefficient and velocity gradient of the fluids. Therefore, the effect of viscous force become larger by the decrease of the diameter corresponding to increase of the velocity gradient (Ma et al., 2020). Hence, during a correlation

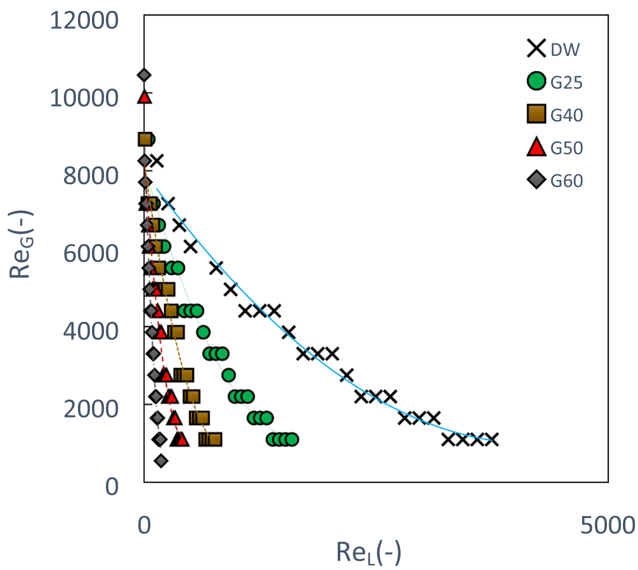

Figure 5. The CCFL characteristics in terms of phase Reynolds numbers

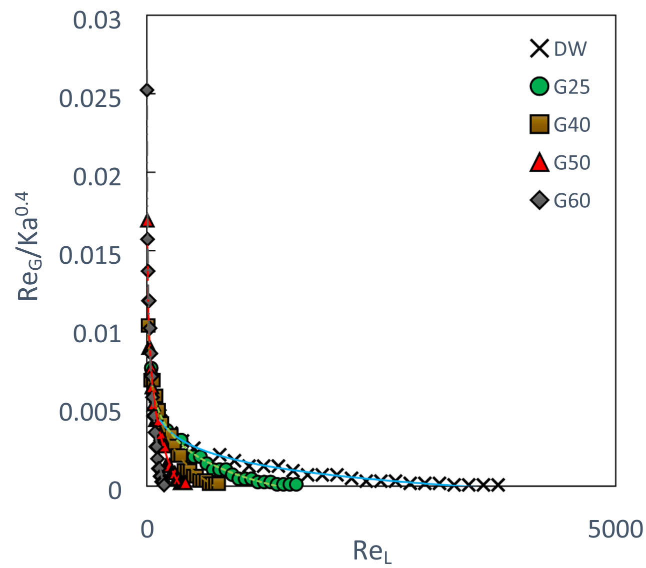

Figure 6. The CCFL characteristics in terms $Re_G/Ka^{0.4}$ against the corresponding liquid Reynold number

development for the typical hot leg geometry, Murase et al. (2012) as well as Kinoshita et al. (2010) also partially reported that the Wallis parameter strongly exhibits the effect of both the liquid viscosity and the channel diameter on the CCFL characteristics.

In conjunction to another geometrical point of view, the difference on characteristic length to diameter (L/D) ratio leads to how long will the regime reach the onset of flooding. Suzuki & Ueda (1977), confirming also the report from McQuilland & Whalley (1985), noticed that flooding gas velocity decreases as the increase of the channel length. Here, Navarro (2005) reported that the gas superficial velocity needed to start pushing the entire liquid decreases with the increase of horizontal length.

Zapke & Kröger (1996) reported that during the investigation of the effect of fluid properties on the CCFL characteristics, the flooding was independent from the gas Reynolds number. They suggested that the non-dimensional superficial gas momentum flux was the one to be correlated during the investigation on CCFL characteristics. On the other hand, Mouza et al. (2003) previously presented a plot of CCFL characteristic in terms of phase Reynolds numbers. They noticed clearly that the slope of the flooding curve depends on the liquid properties as well as the channel diameter.

Figure 5 illustrates the CCFL characteristics of the present data in terms of phase Reynolds numbers. From the figure it can be seen that the flooding gas Reynolds number (Re_G) monotonically decreases with the corresponding liquid Reynolds number (Re_L). Here also, under a given liquid Reynold number, the gas Reynolds number to initiate flooding decreases with the increase of the glycerol percentage of the liquid. Furthermore, the highest glycerol percentage exhibits the largest slope on CCFL characteristic curve. However, the larger gas Reynolds number exhibits the higher gas superficial velocity, while here also, the larger glycerol concentration corresponds to the higher viscosity and the lower surface tension. Therefore, the CCFL characteristic in terms of phase Reynolds numbers also displays similar trend lines, i.e. concave shapes, to that phase superficial velocities obtains. Moreover, the present results are in a fair agreement to that reported by Mouza et al. (2003) in which their CCFL characteristic curve revealed that the liquid with the higher viscosity exhibits the smaller slope while for the same liquid Reynolds number, the gas Reynolds number exhibited to initiate flooding is smaller for the lower surface tension due to both the spreading of lateral liquid and wave formation. Here also, from the figure it can be seen that G60 which corresponds to the highest concentration of glycerol exhibits a very small range of Reynolds number.

In addition, during the investigation the effect of liquid properties on counter-current flow with low Reynolds numbers, considering the theory of stability analysis previously proposed by Cetinbudaklar & Jameson (1969), Mouza et al. (2003) as well as Drosos et al. (2006) attempted to correlate the CCFL data by utilizing gas Froude (Fr_G) and Kapitza (Ka) numbers to the corresponding liquid Froude number. However, they reported that the critical flooding velocities is proportional to the corresponding Kapitza number. Therefore, the applicability of the Kapitza number was proper to be taken into consideration during the investigation of the effects of the liquid properties on the CCFL characteristics (Murase et al., (2012). Here, the Kapitza number, representing the ratio of the surface tension to inertial force, is expressed as written in Eq.(12).

$$Ka = \frac{\sigma}{\mu_L}\left(\frac{\rho_L}{\mu_L g}\right)^{1/3} \tag{12}$$

Here, σ denotes the surface tension, while μ represents the liquid dynamic viscosity. As previously proposed by Ousaka et al. (2006), it is important to include the surface tension to correlate the obtained flooding data. Additionally, Figure 6 depicts the CCFL characteristics in terms of the quantity gas Reynolds to Kapitza $\left(Re_G/Ka^{0.4}\right)$ number against the corresponding liquid Reynolds number, Re_L. The figure shows that $Re_G/Ka^{0.4}$ decreases as the increase in liquid Reynolds number in which the DW obtains the highest trend line among the others. Here as the increase of liquid Reynolds number, smoother decline in $Re_G/Ka^{0.4}$ is obtained. Furthermore, the present result also exhibits a similar trend to the obtained results by both Mouza et al. (2003) and also Drosos et al. (2006) during the investigation of liquid viscosity effect on CCFL characteristics in both vertical and inclined conduits. Additionally, the present experimental data which widely scatter due to the increase of liquid Reynolds number represent that the corresponding numbers are probably inadequate to correlate CCFL characteristics in hot leg geometry.

As described in a report by Zapke & Kröger (2000b), Cetinbudaklar & Jameson (1969) through a theoretical analysis investigated the liquid viscosity effects on the liquid film behavior during two-phase flow. Here, the instability of the liquid film increases with the increase in the viscosity due to the less viscous damping effect at the wall. Furthermore, during a constant liquid flow rate, the higher the viscosity, the smaller the liquid film thickness. They proposed a non-dimensional parameter, i.e. the Ohnesorge number (Oh_L), which increases as the flow instability increases, to indicate the stability of the liquid film draining down the

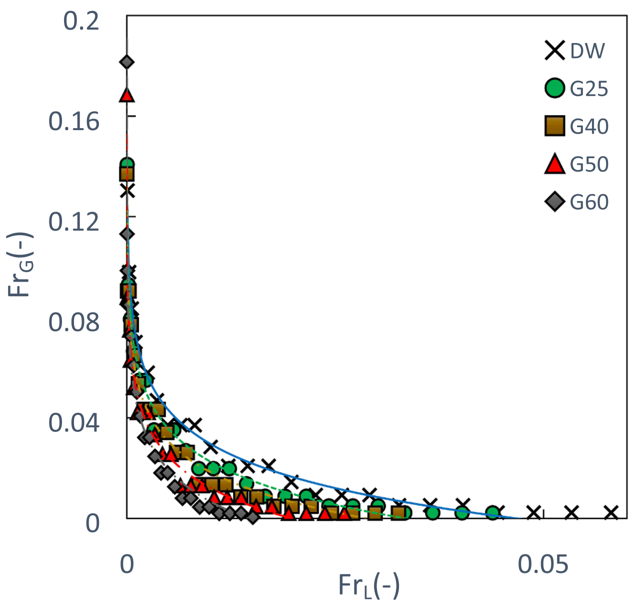

Figure 7. The CCFL characteristics in terms of phase Froude numbers

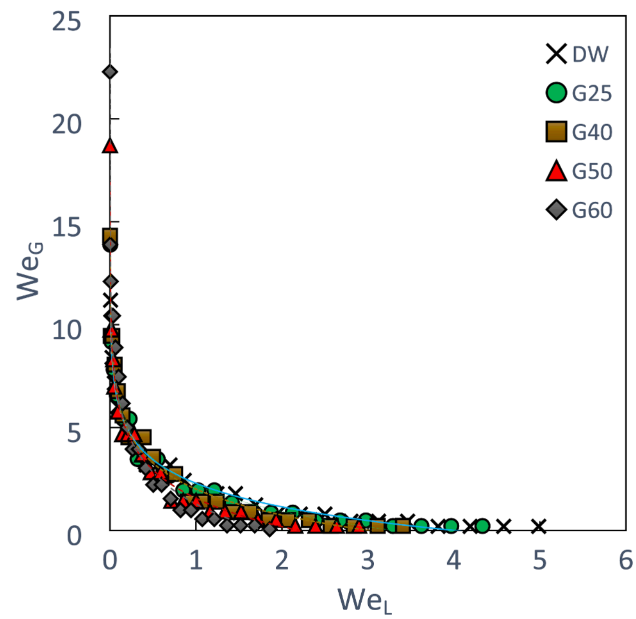

Figure 9. The CCFL characteristics in terms of phase Weber numbers

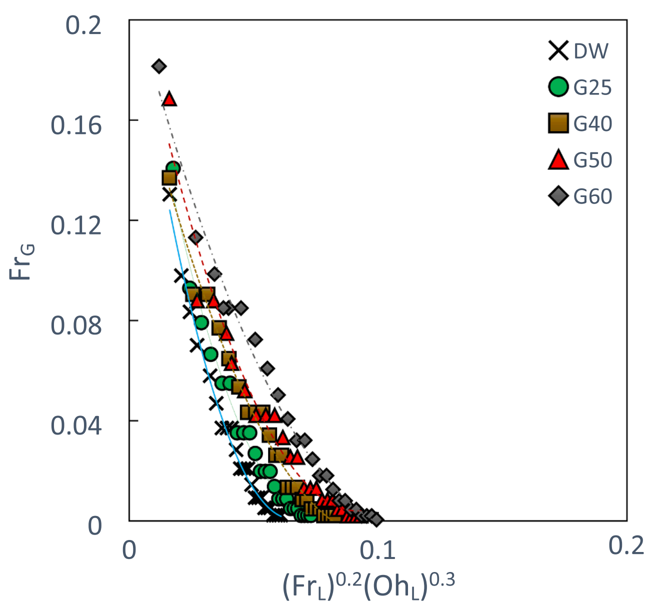

Figure 8. The CCFL characteristics in terms of densimetric liquid Froude and Ohnesorge numbers against the corresponding gas Froude number

conduit wall. In addition, particular stabilizing effect due to the liquid surface tension is also taken into account by this dimensionless number. Therefore, considering that flooding is also governed by the gas Froude number (Fr_G), Zapke & Kröger (2000a) proposed a new correlation for flooding through a modified dimensionless groups connecting the Ohnesorge to liquid Froude number, $(Fr_L)^{0.2}(Oh_L)^{0.3}$. The phase Froude and the liquid Ohnesorge numbers, representing the ratio of inertial to buoyance forces and the liquid viscous to surface tension, respectively, are expressed as written in Eqs.(13) and (14).

$$Fr_K = \frac{\rho_K J_K^2}{gD(\rho_L - \rho_G)} \tag{13}$$

$$Oh_L = \left(\frac{\mu_L^2}{\rho_L D\sigma}\right)^{0.5} \tag{14}$$

Considering that the momentum flux and the liquid density are exhibited in the corresponding phase Froude numbers, and also the effect of the liquid properties on the gas flooding velocity counted by the Ohnesorge number, Deendarlianto et al. (2004) later utilized the proposed non-dimensional number by Zapke & Kröger (1996) on the CCFL data plotted to investigate the effect of surface tension on the flow pattern and CCFL in an inclined pipe. However, they later found that the proposed dimensionless number is not appropriate to predict CCFL in incline channel.

Figure 7 depicts the CCFL characteristics in terms of phase Froude numbers. From the figure it can be seen that the highest trend for flooding gas Froude number is obtained for distilled water. Here, it seems that the gas Froude number decreases with the increase of the percentage of glycerol. A similar trend was previously reported by Zapke & Kröger (2000b) during the addition of the percentage of methanol to the medium water. They strongly noticed that the smallest Ohnesorge number obtained by the pure water exhibits the highest Froude number, and vice versa. The liquid with the highest Ohnesorge number floods at lower gas velocities. Therefore, the gas Froude number at flooding is then a function of the liquid Froude number and the Ohnesorge number.

Moreover, Figure 8 depicts the CCFL characteristics in terms of densimetric phase Froude-Ohnesorge numbers, $(Fr_L)^{0.2}(Oh_L)^{0.3}$, which was proposed by Zapke & Kröger (2000a), and subsequently validated to several previous data obtained by Clift et al. (1966) and Chung et al. (1980) (Zapke & Kröger, 2000b). Furthermore, this non-dimensional group was also utilized by Deendarlianto et al. (2004) during the investigation of the effect of liquid surface tension on CCFL characteristics. The present non-dimensional group was strongly recommended by Zapke & Kröger (2000b) to correlate the flooding data due to the effect of the liquid properties. They proposed that since the Ohnesorge number was an indication of the stability of the liquid film, so that as the Ohnesorge number increases, the liquid viscosity increases, and the liquid film becomes more unstable causing the onset of CCFL to be reached at lower gas flow rates.

In addition, from the figure it is noticed that the present experimental data are not well correlated employing this non-dimensional grouping although the Ohnesorge number, which considers surface tension, is included to the present model. From the finding, it may be concluded that the model, involving the Ohnesorge number, is not sufficient to correlate the CCFL data in the PWR hot leg typical geometry. This result also partially emphasizes the previous finding obtained by

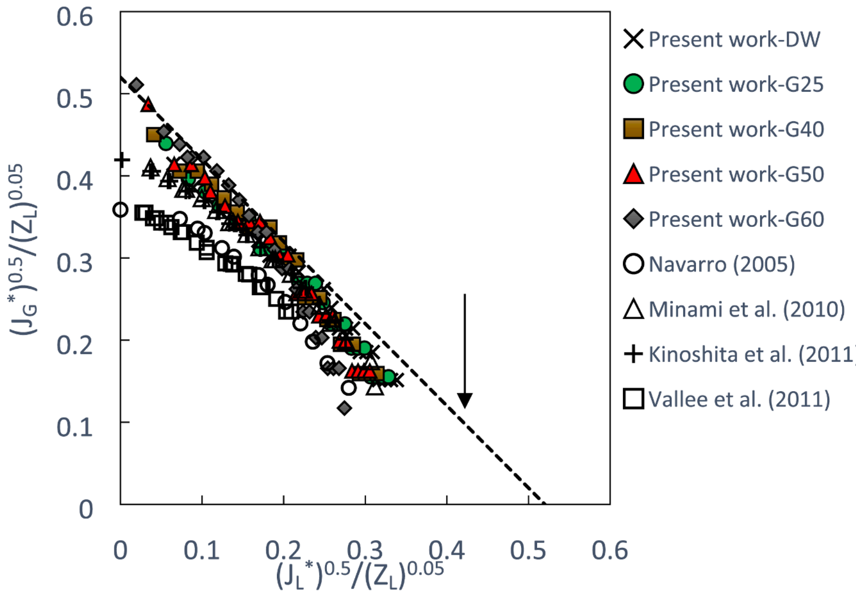

Figure 10. The CCFL characteristics in terms of groups $(J_K^*)^{0.5}/Z_L^{0.05}$ proposed by Zapke & Kröger (1996)

Deendarlianto et al. (2004) in which the current model proposed by Zapke & Kröger (2000a) was found not suitable to be applied during CCFL prediction in inclined pipes. However, as previously also reported by Murase et al. (2012) since the Wallis parameter comprises the influence of the characteristic length, the Ohnesorge number may not be necessary to correlate the CCFL data obtained from hot leg models.

Since the CCFL involves a flow pattern transition, the Weber number (*We*), elucidating the effect of inertia to surface tension in a flow transition, may be considered to correlate the CCFL data due to the different values of surface tension. Here, the Weber number is formulated as written in Eq.(15).

$$We_K = \frac{\rho_K J_K^2 D}{\sigma} \tag{15}$$

Figure 9 illustrates the CCFL characteristics in terms of phase Weber numbers. From the figure it is noticed that the air/distilled water pair elaborates the highest flooding gas Weber number. Here it seems that the flooding gas Weber number decreases with the increase of the percentage of glycerol. It further means that the higher interfacial surface tension, representing by the larger percentage of glycerol, the lower the flooding gas Weber number. Thus, it exhibits similar trends to what was previously exhibited by using the terms of phase Froude numbers as demonstrated in Figure 7. Moreover, in an agreement to the result of Deendarlianto et al. (2004) who previously investigated the effect of liquid surface tension on the flow pattern transition during countercurrent flow in an inclined pipe, the Weber number alone does not satisfactorily correlate the present experimental data.

It is very common to realize that varying one liquid property without affecting the other properties is often not achievable during experiments in which a small variation in the remaining properties obtains another considerable influence (Zapke & Kröger, 1996). Therefore, the liquid property parameter (Z_L), representing the inverse of the Ohnesorge number, is thus proposed considering those relative effects which might be experienced by the flow, and defined as expressed in Eq.(16).

$$Z_L = \frac{(\rho_L D\sigma)^{0.5}}{\mu_L} \tag{16}$$

Figure 10 depicts the CCFL characteristics with respect to the liquid properties in terms of proposed groups, $(J_K^*)^{0.5}/Z_L^{0.05}$, which was previously introduced by Zapke & Kröger (2000b), and also utilized by Prayitno et al. (2012). Those authors reported that the groups are able to indicate the relative effects of the fluid properties on CCFL. Here, the liquid property parameter (Z_L), which takes into account the effect of fluid properties, and the corresponding phase Wallis numbers, is further correlated as written in Eq.(17). (Zapke & Kröger, 1996; Mouza et al., 2003).

$$(J_G^*)^{0.5} + m(J_L^*)^{0.5} = CZ_L^b \tag{17}$$

Moreover, Figure 10 reveals that at low liquid velocities, the larger the concentration of glycerol in the test liquid, which then corresponds to the higher liquid viscosity, the higher the $(J_G^*)^{0.5}/Z_L^{0.05}$ to reach CCFL. On the other hand, at higher liquid flow rates, the larger the percentage of glycerol, the lower $(J_G^*)^{0.5}/Z_L^{0.05}$ to reach CCFL. Furthermore, in a partial agreement to Zapke & Kröger (1996), the group of dimensionless numbers successfully correlates the present experimental data.

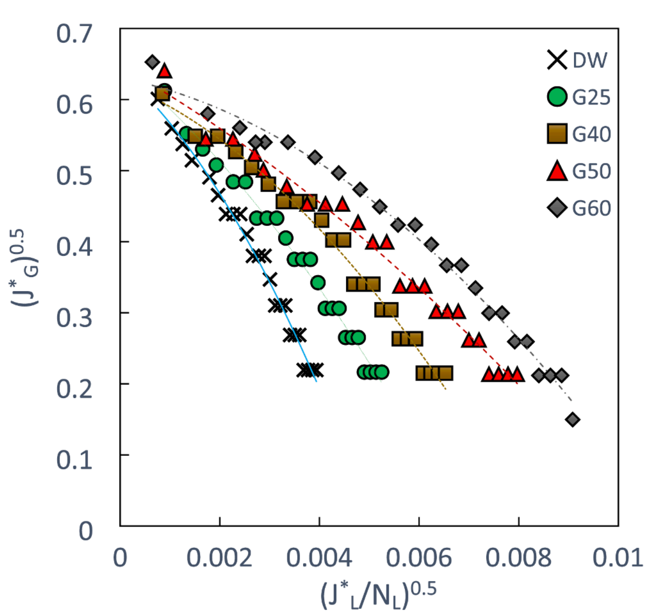

Figure 11. The CCFL characteristics in terms of non-dimensional square root of inverse liquid viscosity against the corresponding gas Wallis parameter

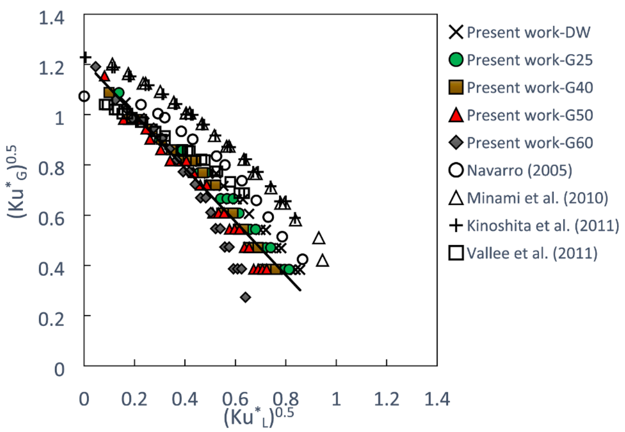

Figure 12. The CCFL characteristics in terms of phase Kutateladze numbers

Therefore, in a partial disagreement with Prayitno et al. (2012), as well as Mouza et al. (2003), it may be concluded that the group appears valid enough to correlate the data obtained from the PWR hot leg model as well as the straight pipes.

Furthermore, the inverse dimensionless viscosity (N_L), as expressed in Eq.(18), during the experimental investigation on the effect of diameter on the horizontal counter-current flow was also proposed by Wallis (1969) and successfully applied by both Ghiaasiaan et al. (1997) and Zapke & Kröger (2000b) to investigate the effect of medium fluid properties, respectively, and also Ma et al. (2020) to identify the influence of diameter on CCFL characteristics. It corresponds to a correction for the Wallis model considering the effects of liquid viscosity, μ_L. Here, during the flow involving high viscous liquid, the liquid inertia was proposed to be proportionally taken into account during the effect of viscous force. Accordingly, the proposed model representing the ratio between the viscous and buoyancy force (Ghiaasiaan et al., 1997) is expressed as shown in Eq.(19).

$$N_L = \frac{\left[D^3 g \rho_L(\rho_L - \rho_G)\right]^{0.5}}{\mu_L} \tag{18}$$

$$\frac{J_L^*}{N_L} = \frac{\mu_L J_L}{gD^2(\rho_L - \rho_G)} \tag{19}$$

Figure 11 presents the CCFL characteristics in terms of liquid Wallis velocity involving the inverse viscosity, $(J_K^*/N_L)^{0.5}$, versus its corresponding gas Wallis velocity. From the figure it is clearly showed that the current model is not sufficient to correlate the present data during the data largely scatter even it comprises the effect of liquid properties to this normalized expression. Furthermore, it was noticed from Ghiaasiaan et al. (1997) that Wallis (1969) proposed that in the vertical conduit, an inertial dominated regime is indicated by $N_L > 300$ during a slug flow. Therefore, it is also implied that CCFL may correspond to an inertial dominated regime in which the viscosity performs a smaller effect rather than the density.

On the other hand, Deendarlianto et al. (2012) clearly remarked that Alekseev et al. (1972), as well as Pushkina & Sorokin (1969), proposed the liquid surface tension (σ) to be considered instead of the diameter (D) to correlate another dimensionless quantity due to the effect of fluid properties. This non-dimensional parameter, well known as the Kutateladze number (Ku_K^*), was derived as the stability of liquid film consideration due to the effect of liquid surface tension, and expressed as written in Eq.(20). Additionally, this non-dimensional number, covering characteristic dimension of gravity (g), surface tension (σ) and phase densities (ρ_K), does not comprise any physical dimension, so although it is reported to be more appropriate for flow in channels free of such effects, such as large-diameter pipes, it mainly does not exhibit the physical effect of the conduit (Zapke & Kröger, 2000a). Therefore, the CCFL characteristics in terms of the phase Kutateladze numbers, corresponding to stability loss of gas/liquid interface, may further be correlated to examine the effect of the fluid properties. Moreover, Mayinger et al. (1993) also reported that the Kutateladze number would be well defined as a scaling parameter for homogeneous flow conditions. Here, the model involving phase Kutateladze number which is defined as the ratio of viscosity to surface tension of liquid is further expressed as written in Eq.(21).

$$Ku_K^* = \frac{J_K(\rho_K)^{0.5}}{\left[g\sigma(\rho_L - \rho_G)\right]^{0.25}} \tag{20}$$

$$\left(Ku_G^*\right)^{0.5} + m\left(Ku_L^*\right)^{0.5} = C \tag{21}$$

Figure 12 describes the CCFL characteristics in terms of phase Kutateladze numbers. It can be seen from the figure that in the range of $0 < \left(Ku_L^*\right)^{1/2} < 0.4$, the curves almost coincide one another. It means that for the mentioned range, an empirical correlation may be raised due to the effect of the liquid properties on the CCFL characteristics. Furthermore, for the entire present experimental data range, applying 20% of relative deviation, the experimental data are also match the boundary, excepted several data obtained from G60. This means that the Kutateladze number gives a better agreement, even though it might not be the most satisfactory approximation. Thus, even though the Kutateladze model had been reported to lost its importance on the literatures during the CCFL in the hot leg geometry, the present result obtains a significant importance of this non-dimensional number. However, the obtained correlation exhibits smaller scattering data rather than the previous correlation utilizing the phase Wallis non-dimensional numbers in the above. Despite during their experiment in a large scale with flat model of hot leg geometry Vallée et al. (2012) concluded that the Kutateladze number failed to correlate the obtained flooding data rather than the Wallis parameter, the present data performs different trend. Moreover, the present result also appears in a partial contrary to what Zapke & Kröger (2000b) previously proposed in which the Kutateladze-type correlation is not applicable for pipe diameters less than 30 mm. In addition, through a linear regression with a $R^2 =$ 0.9243, the present experimental data obtain a formula as written in Eq. (22).

$$\left(Ku_G^*\right)^{0.5} + 0.0938\left(Ku_L^*\right)^{0.5} = 0.1065 \tag{22}$$

However, a report by Mayinger et al. (1993), Hertlein and Herr, (1989), as well as Gleaser (1989) proposed that a modification of the Kutateladze-scaling would be needed for applying to heterogeneous flow conditions. Furthermore, during the consideration of the effect of liquid surface tension, Zapke & Kröger (2000b) proposed the CCFL characteristics in terms of ratio of Kutateladze to Bond number, Bo, which was previously introduced by Chung et al. (1980) as given in the Eq.(23) and Eq.(24), respectively. Again, Zapke & Kröger (2000b) proposed that the combination of the Kutateladze and Bond number also appears not to be able to correlate the obtained experimental data. On the other hand, in the present experimental data, the CCFL characteristic implied from the proposed non-dimensional parameter obtains a similar characteristic to the used of the previous dimensionless number due to the very small effect of the surface tension effect during the present experiment employing water based solution as described previously in Table 1. However, the surface tension effect has been addressed to be smaller with the increase in channel diameter. Therefore, the previous result reported by Ma et al. (2020) that experiments employing larger than 20 mm in diameter, invite a negligible small influence of liquid surface tension has been confirmed.

$$Bo = \frac{gD^2(\rho_L - \rho_G)}{\sigma} \tag{23}$$

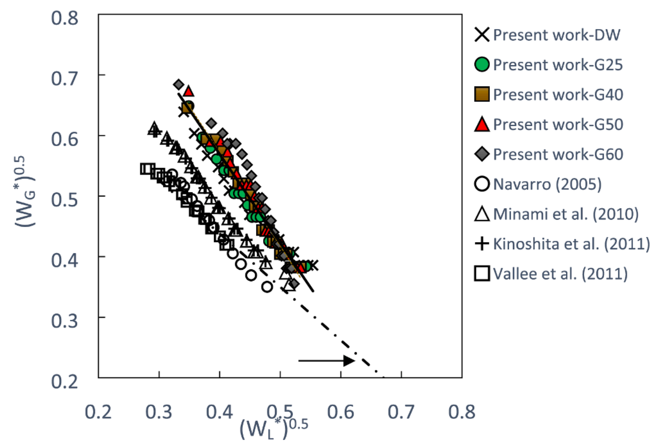

Figure 13. The CCFL characteristics in terms of modified dimensionless Wallis and inverse viscosity proposed by Ma et al. (2020)

$$\left(Ku_G^*\right)^{0.5}+m\left(Ku_L^*\right)^{0.5}=c_1 tanh\left[c_2(Bo)^{0.125}\right] \tag{24}$$

Recently, Ma et al. (2020) proposed a novel non-dimensional model applying the inverse viscosity parameter to the Wallis correlation in order to account for the effect of the diameter on the CCFL characteristics. Here it corresponds to the dimensionless inertia and viscous force, as expressed in Eq.(25), while the developed correlation for $D \ll 100$ mm, accordingly, is formulated as shown in Eq.(26).

$$W_K^*=\left[\frac{\rho_K J_K^2}{gD(\rho_L-\rho_G)}+\left(\frac{\mu_K J_K}{gD^2(\rho_L-\rho_G)}\right)^{0.3}\right]^{0.5} \tag{25}$$

$$\left(W_G^*\right)^{0.5}+0.88\left(W_L^*\right)^{0.5}=0.79 \tag{26}$$

Figure 13 shows the effects of the liquid properties on CCFL characteristics in terms of the square root of the modified non-dimensional Wallis involving the additional of inverse viscosity $(W_K^*)^{0.5}$ as previously proposed by Ma et al. (2020). From the figure it can be seen that even though the novel parameter was basically proposed for the investigation of the effect of diameter on the CCFL characteristics, it is also able to correlate the present experimental data. Comparing to Eq.(21), it is clearly seen that the correlation proposed by Ma et al. (2020) underestimates the present experimental data. Furthermore, by applying $\pm$10% of relative deviation limit, the obtained experimental data mostly match the boundary. Accordingly, through a linear regression with a $R^2 = 0.9368$, the experimental data correlate the CCFL characteristics as written in Eq.(27).

$$\left(W_G^*\right)^{0.5}+1.4538\left(W_L^*\right)^{0.5}=1.2544 \tag{27}$$

However, as earlier noticed, the grouping of non-dimensional numbers proposed by Ma et al. (2020) was derived during the investigation of the influence of the channel's diameter on the CCFL characteristics in straight horizontal pipes. Furthermore, their data were taken from a horizontal configuration of several channels with different diameters. On the other hand, the present experiment was conducted by employing a single-diameter channel with several tested liquids. It further strongly addresses a distinguishable purpose. Thus, even though the effect of liquid properties may be induced on the diameter effect on the CCFL characteristics, other investigations are still pursued to be carried out in order to widely recognize those corresponding models.

3.2. *Dimensional-similarity analysis of present experimental data*

A scientific review accomplished by Deendarlianto et al. (2012) strongly noticed that the existing group of non-dimensional numbers derived for CCFL characteristics in straight channels, comprising either vertical or horizontal conduits, have not taken into consideration the mass exchange between the phases as experienced by the flow in a hot leg typical geometry. Therefore, the hot leg CCFL may embed different characteristics due to different behaviors in the corresponding phenomena. Firstly, in vertical channels with uninterrupted flow, the instability of the interface which initiates CCFL due to the momentum exchange at the interface determines the CCFL trigger with continuous interfaces. On the other hand, here in the hot leg typical geometry, secondary flows within phasic interactions at beyond just a continuous interface are initiated due to the flow experiences an interruption at the bend.

Secondly, the mass flow rate of either phase should be a variable with location in the channel when saturated steam is being condensed as the condensation reduces the mass flow rate and drastically decreases the amount of momentum that the steam is able to transfer to the condensate. As a result, such force ratios previously introduced by those authors in straight channels are not sufficient to predict the hot leg CCFL since the correlations are being used in situations beyond those they were intended for. Therefore, the preceding description further emphasizes the importance on developing alternative empirical models to correlate the experimental data due to the flow nature in the hot leg.

A dimensional-similarities analysis, originally proposed as a method of correlation development during experimental works, is often carried out to exhibit the factors influencing a parameter. It was successfully applied by Juwana et al. (2019) and also Mawarni et al. (2022) during both the estimation of average bubble diameter and the prediction of volumetric mass transfer coefficient in microbubble generator (MBG) systems. Furthermore, Hudaya et al. (2019) as well as Wijayanta and Deendarlianto (2022, in press) developed dimensional analyses to reveal the dominant factor affecting the wave frequency during stratified co-current flow. Moreover, an empirical correlation to estimate the water superficial velocity during the investigation of hydrodynamic behaviors in the airlift pump MBG type was proposed by Catrawedarma et al. (2021).

In the present investigation the authors consider that the gas superficial velocity is the function of the liquid superficial velocity, channel's diameter, both phase densities and dynamic viscosities, liquid surface tension and also the gravitational acceleration. Furthermore, those parameters may be written as shown in Eq.(28), while Table 4 comprises the variables of dimensional analysis.

Table 4
Variables of dimensional analysis.

Variable	Symbol	Dimension Mass	Length	Time
Diameter	D	0	1	0
Density	ρ	1	-3	0
Dynamic viscosity	μ	1	-1	-1
Surface tension	σ	1	0	-2
Gravitational acceleration	g	0	1	-2
Velocity	J	0	1	-1

$$J_G=f(J_L,D,\rho_L,\rho_G,\mu_L,\mu_G,\sigma,g) \tag{28}$$

Taking the pipe diameter D, liquid superficial velocity J_L, and liquid density ρ_L as the repeated variables, those parameter relationships may be then arranged as listed in Eqs.(29) to (34).

$$\Pi_1=\frac{J_G}{J_L} \tag{29}$$

$$\Pi_2=\frac{\rho_G}{\rho_L} \tag{30}$$

Table 5
Non-dimensional numbers utilized to correlate the present flooding data

Non-dimensional number	Symbol	Definition
Reynolds number	*Re*	$\rho JD/\mu$
Kutateladze number	*Ku*	$\rho^{0.5}J/[g\sigma(\rho_L-\rho_G)]^{0.25}$
Bond number	*Bo*	$gD^2(\rho_L-\rho_G)/\sigma$
Weber number	*We*	$\rho J^2D/\sigma$
Froude number	*Fr*	J^2/gD
Mass flux rate	–	$\rho_G J_G/\rho_L J_L$
Density ratio	–	ρ_G/ρ_L
Viscosity ratio	–	μ_G/μ_L

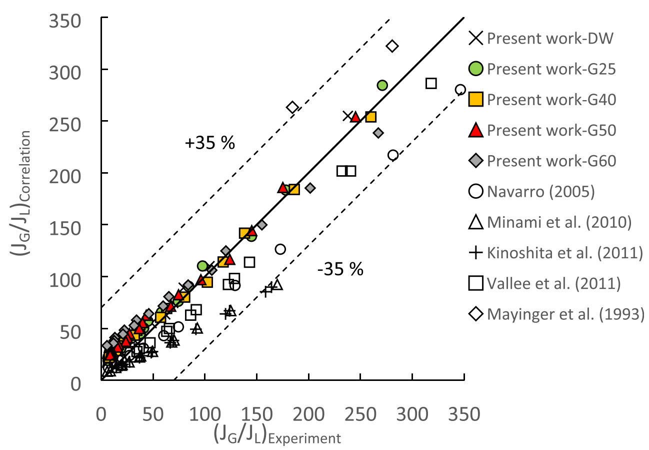

Figure 14. Correlation of the experimental data with Eq. (35)

$$\Pi_3 = \frac{\mu_L}{\rho_L JD} \tag{31}$$

$$\Pi_4 = \frac{\mu_G}{\rho_L J_L D} \tag{32}$$

$$\Pi_5 = \frac{\sigma}{\rho_L J_L^2 D} \tag{33}$$

$$\Pi_6 = \frac{Dg}{J_L^2} \tag{34}$$

Here from Eqs.(29) to (34), it is clearly noticed that the ratio of fluid viscosity will not be included for the purpose of correlating the flooding data. This is also in a partial agreement to what previously reported by Zapke & Kröger (2000b) during the flooding data correlation for vertical and inclined ducts. Moreover, the general form of the parameter relationship is arranged as written in Eqs.(35) to (37).

$$\Pi_1 = f(\Pi_2, \Pi_3, \Pi_4, \Pi_5, \Pi_6) \tag{35}$$

$$\frac{J_G}{J_L} = f\left(\frac{\rho_G}{\rho_L}, \frac{\mu_L}{\rho_L J_L D}, \frac{\mu_G}{\rho_L J_L D}, \frac{\sigma}{\rho_L J_L^2 D}, \frac{Dg}{J_L^2}\right) \tag{36}$$

$$\left(\frac{J_G}{J_L}\right) = a\left(\frac{\rho_G}{\rho_L}\right)^b \left(\frac{\mu_L}{\rho_L J_L D}\right)^c \left(\frac{\mu_G}{\rho_L J_L D}\right)^d \left(\frac{\sigma_L}{\rho_L J_L^2 D}\right)^e \left(\frac{Dg}{J_L^2}\right)^f \tag{37}$$

In addition, several groups obtained above elaborate several well-known numbers as listed in Table 5, while the coefficient constant a, b, c, d, e, f are obtained by curve fitting through the tabulated experimental data. Accordingly, from the fitting, we obtain the constants as written in Eq.(38).

$$\left(\frac{J_G}{J_L}\right) = 0.95\left(\frac{\rho_G}{\rho_L}\right)^{0.1} (Re_L)^{0.1} \left(\frac{\mu_G}{\rho_L J_L D}\right)^{0.05} (We_L)^{0.05} (Fr_L)^{-0.8} \tag{38}$$

Here the correlation as expressed in Eq.(38) implies that the inverse liquid Froude number obtains the highest effect on the phase superficial velocity ratio by the power of 0.8, while the liquid Weber number obtains the lowest by the power of 0.05. On the other hand, the superficial velocity ratio is proportional to $\mu_L{}^{0.1}$ due to the liquid viscosity is only included in the liquid Reynolds number (-0.1 power). Subsequently, the superficial velocity ratio is also proportional to $\sigma_L{}^{0.05}$ since the liquid surface tension is only comprised in the liquid Weber number (-0.05 power). Therefore, the developed correlation notices that the liquid viscosity obtains higher effect rather than its surface tension. The present result is in a partial agreement to what reported by Suzuki & Ueda (1977).

Moreover, Figure 14 presents the correlation of the experimental data with Eq.(38). From the figure, it is implied that by the relative deviation of ±35 %, the developed correlation fairly estimated the flooding superficial velocity ratio. Accordingly, in a comparison to previously experimental data obtained by other authors, the present empirical correlation over predict the data obtained by Navarro (2005), Kinoshita et al. (2011), and Vallée et al. (2011). Taking into account that the present experiment was carried out in a 1/30 scaled-down geometry whereas Vallée et al. (2011) and Kinoshita et al. (2011) as well as Navarro (2005) employed 1/15 scaled-down model. Here, the scale model probably exhibits a distinguished aspect. However, the present developed correlation notices that the pipe diameter which is still covered in the liquid Reynolds number (0.1 power), $\mu_G/\rho_L J_L D$ (-0.05 power), liquid Weber number (0.05 power), and liquid Froude number (0.8 power) obtains the highest power, in which the superficial velocity ratio is proportional to $D^{0.9}$ (0.1 - 0.05 + 0.05 + 0.8 = 0.9).

3.3. Uncertainty analysis

The accuracy of volumetric flow rate measurements may cause experimental uncertainty. In the present work, the measured quantities were evaluated according to Moffat (1988). Similar analyses were previously reported by Wongwises (1994) on investigation of flooding in counter-current flow, and also Catrawedarma et al. (2022) during the study of hydrodynamic behaviors of air/water two-phase flow in water lifting in a bubble generator type of airlift pump system. In the present work, the uncertainty analysis covers the uncertainty in both gas and liquid flow measurements. In the gas flow rate measurement, the correlation provided by the flow meter manufacturer is given in Eq.(39).

$$Q_{AG} = Q_{RG}\sqrt{\frac{P_g}{P_a}\frac{T_a}{T_f}} \tag{39}$$

Taking into account an adiabatic system during the data tabulation, the ambient temperature (T_a) is then considered the same as the gas temperature (T_f). Therefore, the Eq.(39) may be further expressed as written in Eq.(40).

$$Q_G = Q_{RG}\sqrt{\frac{P_g}{P_a}} \tag{40}$$

Here in the Eq.(40), the actual gas volumetric flow rate (Q_G) is a function of the reading volumetric flow rate (Q_{RG}) and the pressure maintained by air pressure regulator (P_g), and may be expressed as shown in Eq.(41).

$$Q_G = f(Q_{RG}, P_g) \tag{41}$$

According to Moffat (1988), a measured quantity on the Eq.(41) can be written as expressed in Eq.(42).

$$\sigma_{Q_G} = \pm\sqrt{\left(\frac{\partial Q_G}{\partial Q_{RG}}\sigma Q_{RG}\right)^2 + \left(\frac{\partial Q_G}{\partial P_g}\sigma P_g\right)^2} \tag{42}$$

Solving Eq.(42), then the uncertainty of gas volumetric flow rate (σ_{Q_G}) as expressed in Eq.(43) is obtained.

Table 6
Test matrix and uncertainties of the experimental results

Test liquid	$Q_{L,corrected}$ (gph)	J_L (m/s)	Uncertainties of Q_L (%)	$Q_{G,corrected}$ (lpm)	J_G (m/s)	Uncertainties of J_G (%)
DW	2.13 - 57.95	0.0044 - 0.1202	1.47 - 6.5	21.1 - 158.6	0.69 - 5.22	7.48 - 7.59
G25	1.45 - 50.37	0.0030 - 0.1045	1.71 - 9.74	21.1 - 169.2	0.69 - 5.57	7.48 - 7.59
G40	0.73- 43.40	0.0015 - 0.0900	1.95 - 13.5	21.1 - 169.2	0.69 - 5.57	7.48 - 7.59
G50	0.48 - 38.83	0.0010 - 0.0805	1.45 - 13.2	21.1 - 190.3	0.69 - 6.26	7.48 - 7.59
G60	0.15 - 29.57	0.0003 - 0.0613	1.56 - 9.45	10.6 - 200.9	0.35 - 6.61	7.48 - 7.89

$$\sigma_{Q_G} = \pm\sqrt{\left(\frac{1.5708 Q_{RG}}{P_g^{\,0.5}}\sigma_{Q_{RG}}\right)^2 + \left(3.1415 P_g^{\,0.5}\sigma_{P_g}\right)^2} \tag{43}$$

On the other hand, in the liquid volumetric flow rate measurement, the actual volumetric flow rate is measured employing a measurement glass and a timer. Thus, the obtained liquid volumetric flow rate is the measured volume divided by the time as expressed in Eq.(44).

$$Q_{AL} = \frac{V_{AL}}{t} \tag{44}$$

Here in the Eq.(44), since the actual liquid volumetric flow rate (Q_{AL}) is a function of the reading volumetric liquid flow rate (V_{AL}) and the time (t), and the corresponding equation may be further expressed as shown in Eq.(45).

$$Q_{AL} = f(V_{AL}, t) \tag{45}$$

Accordingly, a measured quantity corresponding to the uncertainty of actual liquid flow rate ($\sigma_{Q_{AL}}$) can be obtained as expressed in Eq.(46).

$$\sigma_{Q_{AL}} = \pm\sqrt{\left(\frac{\partial Q_{AL}}{\partial V_{AL}}\sigma_{V_{AL}}\right)^2 + \left(\frac{\partial Q_{AL}}{\partial t}\sigma_t\right)^2} \tag{46}$$

Solving Eq.(46), then then the uncertainty of actual liquid volumetric flow rate ($\sigma_{Q_{AL}}$) as expressed in Eq.(47) is obtained.

$$\sigma_{Q_{AL}} = \pm\sqrt{\left(\frac{1}{t}\sigma_{V_{AL}}\right)^2 + \left(\frac{-V_{AL}}{t^2}\sigma_t\right)^2} \tag{47}$$

Moreover, the liquid flowmeter reading (Q_{RL}) also invites an uncertainty. Therefore, utilizing a linier regression, the relation between the reading and the actual liquid flowrate (Q_{AL}) can be obtained by its correlation gradient (m), and expressed as written in Eq.(48) & (49).

$$Q_{AL} = mQ_{RL} + c \tag{48}$$

$$m = f(Q_{AL}, Q_{RL}) \tag{49}$$

Accordingly, the measured quantity corresponding to the uncertainty of correlation gradient (σ_m) can be written as expressed in Eq.(50).

$$\sigma_m = \pm\sqrt{\left(\frac{\partial m}{\partial Q_{AL}}\sigma_{Q_{AL}}\right)^2 + \left(\frac{\partial m}{\partial Q_{RL}}\sigma_{Q_{RL}}\right)^2} \tag{50}$$

Solving Eq.(50), then Eq.(51) is obtained.

$$\sigma_m = \pm\sqrt{\left(\frac{\sigma_{Q_{AL}}}{Q_{RL}}\right)^2 + \left(\frac{c\sigma_{Q_{RL}}}{Q_{RL}^{\,2}} - \frac{Q_{AL}\sigma_{Q_{RL}}}{Q_{RL}^{\,2}}\right)^2} \tag{51}$$

Therefore, the total uncertainty of liquid volumetric flow rate (σ_{Q_L}) is formulated as expressed in Eq.(52).

$$\sigma_{Q_L} = \pm\sqrt{\left(\frac{1}{t}\sigma_{V_{AL}}\right)^2 + \left(\frac{-V_{AL}}{t^2}\sigma_t\right)^2 + \left(\frac{\sigma_{Q_{AL}}}{Q_{RL}}\right)^2 + \left(\frac{c\sigma_{Q_{RL}}}{Q_{RL}^{\,2}} - \frac{Q_{AL}\sigma_{Q_{RL}}}{Q_{RL}^{\,2}}\right)^2} \tag{52}$$

Moreover, Table 6 provides the quantities of uncertainty combined with the listing of flow range. Herein, except for the smallest liquid volumetric flow rate delivered by both the air/G40 and air/G50 flow, the uncertainties of Q_L are mostly less than 10%. On the other hand, the uncertainties of Q_G are less than 8%.

4. Concluding remarks

An attempt to reveal the influence of the liquid properties on the CCFL characteristics in the German Konvoi PWR hot leg was carried out. Experiments were conducted with five test liquids in a 1/30-scale facility. From analysis of these data, the main conclusions are as follows:

1. The gas flow rate needed to initiate the flooding monotonically decreases as the liquid flow rate increases. In the higher liquid flow rates, adding the concentration of glycerol into the test liquid increases the sensitivity of flooding initiation to the gas flow rate. Here, under a given flow condition, the onset of flooding is obtained faster by a higher glycerol concentration.
2. Instead of the well-known phasic Wallis parameters, Kutateladze-type numbers, or the group of Wallis-liquid property by Zapke & Kröger (1996), a modified non-dimensional phasic Wallis parameter involving inverse viscosity numbers introduced by Ma et al. (2020) shown to better correlate the present experimental data with respect to the effect of liquid properties on CCFL characteristics.
3. The proposed empirical correlation obtained from the present data implies that due to the effect of liquid properties, the viscosity exhibits greater influence on CCFL than the corresponding surface tension.
4. The finding of the present work provides extensive database of the critical conditions leading to CCFL considering the effect of liquid properties to assess the significance of non-dimensional groups employed for CCFL correlation. A developed empirical correlation to predict the flooding gas to liquid superficial velocity ratio is addressed in conjunction with theoretical modeling to develop necessary and sufficient groups of non-dimensional numbers to correlate the CCFL data. It further enhances the understanding of the role of liquid property allows for better accuracy in analysis to promote extended operation and improve the reactor safety.

CRediT authorship contribution statement

Achilleus Hermawan Astyanto: Conceptualization, Methodology, Investigation, Writing – original draft, Formal analysis. **Indarto:** Resources, Funding acquisition, Writing – review & editing, Supervision. **Karen Vierow Kirkland:** Methodology, Formal analysis, Writing – review & editing. **Deendarlianto:** Resources, Funding acquisition, Supervision, Conceptualization, Methodology, Validation, Writing – review & editing.

Declaration of Competing Interest

The authors declare that they have no known competing financial interests or personal relationships that could have appeared to influence the work reported in this paper.

Data availability

Data will be made available on request.

Acknowledgment

Regarding the funding of a research framework through both the Beasiswa Pendidikan Pascasarjana Dalam Negeri (BPPDN) 2019 and the secondary annum of Penelitian Desertasi Doktor (PDD) 2021 (contract number: 2303/UN1/DITLIT/DIT-LIT/PT/2021), the authors acknowledge both Direktorat Pendidikan Tinggi (DIKTI) and Direktorat Riset dan Pengabdian Masyarakat (DRPM) Kementerian Pendidikan, Kebudayaan, Riset dan Teknologi (KEMENDIKBUD-RISTEK) Republic of Indonesia. Here also, for either several brief discussions during the apparatus design & manufacturing as well as the image & signal processing methodology or the data tabulation assistances, we thank Dr. Apip Badarudin, Dr. I Gusti Ngurah Bagus Catrawedarma, Dr. Setya Wijayanta, Mr. Akhlisa Nadiantya Aji Nugroho, Mr. Alfikri Ihsan, Mr. Andhika Satria Pratama, Mrs. Yulia Venti Yoanita, and also Mrs. Christina Deni Rumiarti. Additionally, during the better perspectives on the flow structure phenomenology, the visual materials were largely captivated utilizing a Phantom Miro Lab310 HSVC. Therefore, we appreciate Chevron Indonesia for the appropriate opportunities.

References

Al Issa, S., Macian-Juan, R., 2014. Experimental investigation of countercurrent flow limitation (CCFL) in a large-diameter hot-leg geometry: A detailed description of CCFL mechanisms, flow patterns and high-quality HSC imaging of the interfacial structure in a 1/3.9 scale of PWR geometry. Nucl. Eng. Des. 280, 550–563. https://doi.org/10.1016/j.nucengdes.2014.08.021.

Ardron, K.H., Banerjee, S., 1986. Flooding in an elbow between a vertical and a horizontal or near-horizontal pipe. Part II: Theory. Int. J. Multiph. Flow 12 (4), 543–558. https://doi.org/10.1016/0301-9322(86)90059-5.

Astyanto, A.H., Pramono, J.A.E., Catrawedarma, I.G.N.B., Deendarlianto, Indarto, 2022. Statistical characterization of liquid film fluctuations during gas-liquid two-phase counter-current flow in a 1/30 scaled-down test facility of a pressurized water reactor (PWR) hot leg. Ann. Nucl. Energy 172, 109065. https://doi.org/10.1016/j.anucene.2022.109065.

Astyanto, A.H., Rahman, Y., Adhikara, A.Y., Indarto, Deendarlianto, 2021a. Time-series differential pressure fluctuations of a flooding regime : A preliminary experimental results investigation on a 1 / 30 down- scaled PWR hot leg geometry. AIP Conf. Proc. 060001 (2011).

Astyanto, A. H., Rahman, Y., Medha, A. Y. A., Deendarlianto, & Indarto. (2021). Pengaruh Rasio I/D terhadap Permulaan Flooding dan Fluktuasi Voltase Sinyal Tekanan Rezim Flooding pada Geometri Kompleks. *Rekayasa Mesin*, *12*(August), 447–457. https://doi.org/https://doi.org/10.21776/ub.jrm.2021.012.02.21.

Badarudin, A., Pinindriya, S. T., Yoanita, Y. V., Hadipranoto, M. S., Hartono, S., Ariawan, R., Indarto, & Deendarlianto. (2018). The effect of horizontal pipe length to the onset of flooding position on the air-water counter current two-phase flow in a 1/30 scale of pressurized water reactor (PWR). *AIP Conference Proceedings*, *2001*(June 2020). https://doi.org/10.1063/1.5049983.

Badarudin, A., Indarto, D., Setyawan, A., 2016. Characteristics of the air-water counter current two-phase flow in a 1/30 scale of pressurized water reactor (PWR): Interfacial behavior and CCFL data. AIP Conf. Proc. 1737 https://doi.org/10.1063/1.4949303.

Badarudin, A., Setyawan, A., Dinaryanto, O., Widyatama, A., Indarto, Deendarlianto, 2018b. Interfacial behavior of the air-water counter-current two-phase flow in a 1/30 scale-down of pressurized water reactor (PWR) hot leg. Ann. Nucl. Energy 116, 376–387. https://doi.org/10.1016/j.anucene.2018.03.007.

Catrawedarma, I., Deendarlianto, Indarto, 2021. Hydrodynamic behaviors of air–water two-phase flow during the water lifting in a bubble generator type of airlift pump system. Heat and Mass Transfer/Waerme- Und Stoffuebertragung 0123456789. https://doi.org/10.1007/s00231-021-03157-z.

Cetinbudaklar, A.G., Jameson, G.J., 1969. The mechanism of flooding in vertical countercurrent two-phase flow. Chem. Eng. Sci. 24 (11), 1669–1680. https://doi.org/10.1016/0009-2509(69)87032-6.

Choi, K.Y., No, H.C., 1995. Experimental studies of flooding in nearly horizontal pipes. Int. J. Multiph. Flow 21 (3), 419–436. https://doi.org/10.1016/0301-9322(94)00087-Z.

Chung, K.S., Liu, C.P., Tien, C.L., 1980. Flooding in two-phase countercurrent flows–II: Experimental investigation. PhysicoChem. Hydrodynam 1, 209–220.

Clift, R., Pritchard, C.L., Nedderman, R.M., 1966. The effect of viscosity on the flooding conditions in wetted wall columns. Chem. Eng. Sci. 21 (1), 87–95. https://doi.org/10.1016/0009-2509(66)80009-X.

Deendarlianto, Höhne, T., Lucas, D., & Vierow, K. (2012). Gas-liquid countercurrent two-phase flow in a PWR hot leg: A comprehensive research review. *Nucl. Eng. Design*, *243*(2), 214–233. https://doi.org/10.1016/j.nucengdes.2011.11.015.

Deendarlianto, Ousaka, A., Indarto, Kariyasaki, A., Lucas, D., Vierow, K., Vallee, C., & Hogan, K. (2010). The effects of surface tension on flooding in counter-current two-phase flow in an inclined tube. *Exp. Therm. Fluid Sci.*, *34*(7), 813–826. https://doi.org/10.1016/j.expthermflusci.2010.01.010.

Deendarlianto, Ousaka, A., Kariyasaki, A., Fukano, T., & Konishi, M. (2004). The Effects of Surface Tension on the Flow Pattern and Counter-Current Flow Limitation (CCFL) in Gas-Liquid Two-Phase Flow in an Inclined Pipe. *Japan. J. Multiphase Flow*, *18*(4), 337–350.

Deendarlianto, Vallée, C., Lucas, D., Beyer, M., Pietruske, H., & Carl, H. (2011). Erratum: Experimental study on the air/water counter-current flow limitation in a model of the hot leg of a pressurized water reactor (Nuclear Engineering and Design). *Nucl. Eng. Design*, *241*(8), 3359–3372. https://doi.org/10.1016/j.nucengdes.2011.02.028.

Diehl, J.E., Koppany, C.R., 1969. Flooding velocity correlation for gas–liquid counterflow in vertical tubes. Chem. Engng Sci 21, 77–83.

Drosos, E.I.P., Paras, S.V., Karabelas, A.J., 2006. Counter-current gas-liquid flow in a vertical narrow channel-Liquid film characteristics and flooding phenomena. Int. J. Multiph. Flow 32 (1), 51–81. https://doi.org/10.1016/j.ijmultiphaseflow.2005.07.005.

Ghiaasiaan, S.M., Wu, X., Sadowski, D.L., Abdel-Khalik, S.I., 1997. Hydrodynamic characteristics of counter-current two-phase flow in vertical and inclined channels: Effects of liquid properties. Int. J. Multiph. Flow 23 (6), 1063–1083. https://doi.org/10.1016/s0301-9322(97)00027-x.

Gleaser, H. Analysis of downcomer and tie plate countercurrent flow in the Upper Plenum Test Facility (UPTF). *Proceeding Fourth International Topical Meeting on Nuclear Reactor Thermal Hydraulics (NURETH-4)*, vol. 1, pp. 75–81, Karlsruhe, October 1989.

Hertlein R. & Herr, W. A new model for countercurrent flow in the upper part of a PWR core, presented at the *Fourth International Topical Meeting on Nuclear Reactor Thermal-Hydraulics*, Karlsruhe, FRG, 10–13, October 1989.

Hudaya, A.Z., Widyatama, A., Dinaryanto, O., Juwana, W.E., Indarto, & Deendarlianto., 2019. The liquid wave characteristics during the transportation of air-water stratified co-current two-phase flow in a horizontal pipe. Exp. Therm Fluid Sci. 103 (January), 304–317. https://doi.org/10.1016/j.expthermflusci.2019.01.021.

Juwana, W.E., Widyatama, A., Dinaryanto, O., Budhijanto, W., Indarto, & Deendarlianto., 2019. Hydrodynamic characteristics of the microbubble dissolution in liquid using orifice type microbubble generator. Chem. Eng. Res. Des. 141, 436–448. https://doi.org/10.1016/j.cherd.2018.11.017.

Kang, S.-K., Chu, I.-C., No, H.C., Chun, M.-H., 1999. Air-Water Countercurrent Flow Limitation in a Horizontal Pipe Connected to an Inclined Riser. Journal of the Korean Nuclear Society 31 (6), 548–560. https://doi.org/10.1080/01457630600793897.

Kim, H.T., No, H.C., 2002. Assessment of RELAP5/MOD3.2.2γ against flooding database in horizontal-to-inclined pipes. Ann. Nucl. Energy 29 (7), 835–850. https://doi.org/10.1016/S0306-4549(01)00074-3.

Kinoshita, I., Murase, M., Utanohara, Y., Minami, N., 2010. Numerical Simulation of Countercurrent Gas- Liquid Flow in a PWR Hot Leg under Reflux Cooling Numerical Simulation of Countercurrent Gas-Liquid Flow. J. Nucl. Sci. Technol. 47 (10), 963–972. https://doi.org/10.1080/18811248.2010.9720975.

Kinoshita, I., Nriai, T., Tomiyama, A., Lucas, D., Murase, M., 2011. Effects of Liquid Properties on CCFL in a Scaled-Down Model of a PWR Hot Leg. Journal of Power and Energy Systems 5 (3), 316–329. https://doi.org/10.1299/jpes.5.316.

Kusunoki, T., Murase, M., Fujii, Y., Nozue, T., Hayashi, K., Hosokawa, S., Tomiyama, A., 2015. Effects of fluid properties on CCFL characteristics at a vertical pipe lower end. J. Nucl. Sci. Technol. 52 (6), 887–896. https://doi.org/10.1080/00223131.2014.990533.

Ma, Y., Shao, J., Lyu, J., Peng, J., 2020. Experimental study on the effect of diameter on gas–liquid CCFL characteristics of horizontal circular pipes. Nucl. Eng. Des. 364 (516), 110645 https://doi.org/10.1016/j.nucengdes.2020.110645.

Mawarni, D.I., Juwana, W.E., Yuwana, K.A., Budhijanto, W., Deendarlianto, Indarto., 2022. Journal of Water Process Engineering Hydrodynamic characteristics of the microbubble dissolution in liquid using the swirl flow type of microbubble generator. J. Water Process Eng. 48 (2), 102846 https://doi.org/10.1016/j.jwpe.2022.102846.

Mayinger, F., Weiss, P., Wolfert, K., 1993. Two-phase flow phenomena in full-scale reactor geometry. Nucl. Eng. Des. 145 (1–2), 47–61. https://doi.org/10.1016/0029-5493(93)90058-H.

McQuilland, K.W., Whalley, P.B., 1985. Flooding in vertical two-phase flow. Int. J. Multiphase Flow 11 (6), 741–760.

Minami, N., Nishiwaki, D., Nariai, T., Tomiyama, A., Murase, M., 2010. Countercurrent gas-liquid flow in a pwr hot leg under reflux cooling (i) air-water tests for 1/15-scale model of a pwr hot leg. J. Nucl. Sci. Technol. 47 (2), 142–148. https://doi.org/10.1080/18811248.2010.9711938.

Moffat, R.J., 1988. Describing the uncertainties in experimental results. Exp. Therm Fluid Sci. 1 (1), 3–17. https://doi.org/10.1016/0894-1777(88)90043-X.

Mouza, A.A., Paras, S.V., Karabelas, A.J., 2003. Incipient flooding in inclined tubes of small diameter. Int. J. Multiph. Flow 29 (9), 1395–1412. https://doi.org/10.1016/S0301-9322(03)00124-1.

Murase, M., Tomiyama, A., Lucas, D., Kinoshita, I., Utanohara, Y., Yanagi, C., 2012. Correlation for countercurrent flow limitation in a PWR hot leg. J. Nucl. Sci. Technol. 49 (4), 398–407. https://doi.org/10.1080/00223131.2012.669241.

Navarro, M.A., 2005. Study of countercurrent flow limitation in a horizontal pipe connected to an inclined one. Nucl. Eng. Des. 235 (10–12), 1139–1148. https://doi.org/10.1016/j.nucengdes.2005.02.010.

Ohnuki, A., 1986. Experimental study of counter-current two-phase flow in horizontal tube connected to inclined riser. J. Nucl. Sci. Technol. 23 (3), 219–232. https://doi.org/10.1080/18811248.1986.9734975.

Ousaka, A., Deendarlianto, K., A., & Fukano, T., 2006. Prediction of flooding gas velocity in gas-liquid counter-current two-phase flow in inclined pipes. Nucl. Eng. Des. 236 (12), 1282–1292. https://doi.org/10.1016/j.nucengdes.2005.12.001.

Pratama, A.S., Indarto, & Deendarlianto., 2021. Studi CFD mengenai Pengaruh Sifat Fisis Fluida terhadap Karakteristik Counter-Current Flow Limitation pada Pipa

Horizontal. Journal of Mechanical Design and Testing 3 (2), 118. https://doi.org/10.22146/jmdt.66408.

Prayitno, S., Santoso, R.a., Deendarlianto, Höhne, T., Lucas, D., 2012. Counter current flow limitation of gas-liquid two-phase flow in nearly horizontal pipe. Sci. Technol. Nucl. Installat. 2012 https://doi.org/10.1155/2012/513809.

Siddiqui, H., Banerjee, S., Ardron, K.H., 1986. Flooding in a N Elbow Between a Vertical a N D a Horizontal or Near-Horizontal Pipe. Int. J. Multiph. Flow 12 (4), 531–541.

Suzuki, S., Ueda, T., 1977. Behaviour of liquid films and flooding in counter-current two-phase flow-Part 1. Flow in circular tubes. Int. J. Multiph. Flow 3 (6), 517–532. https://doi.org/10.1016/0301-9322(77)90027-1.

Utanohara, Y., Kinoshita, I., Murase, M., Lucas, D., Vallée, C., Tomiyama, A., 2012. Numerical simulations for steam-water CCFL tests using the 1/3 scale rectangular channel simulating a PWR hot leg. Nucl. Eng. Des. 249, 14–23. https://doi.org/10.1016/j.nucengdes.2011.05.041.

Vallée, C., Seidel, T., Lucas, D., Beyer, M., Prasser, H.M., Pietruske, H., Schütz, P., Carl, H., 2012. Counter-current flow limitation in a model of the hot leg of a PWR - Comparison between air/water and steam/water experiments. Nucl. Eng. Des. 245, 113–124. https://doi.org/10.1016/j.nucengdes.2012.01.001.

Vallée, C., Seidel, T., Lucas, D., Tomiyama, A., Murase, M., 2011. Comparison of countercurrent flow limitation experiments performed in two different models of the hot leg of a pressurized water reactor with rectangular cross section. J. Eng. Gas Turbines Power 133 (5), 1–9. https://doi.org/10.1115/1.4002884.

Vierow, K., Mohammed, N., & Aumiller, D. (2015). Effects of steam-water vs. air-water fluid pairs and pressure on flooding in large-diameter tubes. *International Topical Meeting on Nuclear Reactor Thermal Hydraulics 2015, NURETH 2015*, *7*, 5573–5586.

Wallis, G.B., 1961. Flooding velocities for Air and Water in Vertical Tubes. UKAEA, Harwell, England. AAEW-R123,.

Wallis, G.B., 1969. One-dimensional Two-phase Flow. McGraw Hill, New York.

Wijayanta, S., Deendarlianto, I., 2022. The effect of the liquid physical properties on the wave frequency and wave velocity of co-current gas-liquid stratified two-phase flow in a horizontal pipe. International Journal of Multiphas Flow. article in press.

Wongwises, S., 1996. Two-phase countercurrent flow in a model of a pressurized water reactor hot leg. Nucl. Eng. Des. 166, 121–133. https://doi.org/10.1016/j.nucengdes.2010.08.016.

Zapke, A., Kröger, D.G., 1996. The influence of fluid properties and inlet geometry on flooding in vertical and inclined tubes. Int. J. Multiph. Flow 22 (3), 461–472. https://doi.org/10.1016/0301-9322(95)00076-3.

Zapke, A., Kröger, D.G., 2000a. Countercurrent gas-liquid flow in inclined and vertical ducts - I: Flow patterns, pressure drop characteristics and flooding. Int. J. Multiph. Flow 26 (9), 1439–1455. https://doi.org/10.1016/S0301-9322(99)00097-X.

Zapke, A., Kröger, D.G., 2000b. Countercurrent gas-liquid flow in inclined and vertical ducts - II: The validity of the Froude-Ohnesorge number correlation for flooding. Int. J. Multiph. Flow 26 (9), 1457–1468. https://doi.org/10.1016/S0301-9322(99)00098-1.